Maximum Bubble Pressure Method: Universal Surface Age and Transport Mechanisms in Surfactant Solutions

Nikolay C. Christov,[†] Krassimir D. Danov,[†] Peter A. Kralchevsky,*[,†]
Kavssery P. Ananthapadmanabhan,[‡] and Alex Lips[‡]

Laboratory of Chemical Physics & Engineering, Faculty of Chemistry, University of Sofia, 1164 Sofia, Bulgaria, and Unilever Research & Development, Trumbull, Connecticut 06611

Received May 3, 2006. In Final Form: June 6, 2006

Here, based on the theoretical analysis of results for two ionic surfactants, sodium dodecyl sulfate (SDS) and dodecyl trimethylammonium bromide (DTAB), we develop a new approach for quantitative interpretation of data from the maximum bubble pressure method. A given tensiometer is characterized by an apparatus function, $A(t)$, and by an apparatus constant. The former represents the time dependence of the bubble surface area, whereas the latter is expressed through integrals of $A(t)$. The experiment indicates that both of them are independent of the surfactant type and concentration. Moreover, if a certain criterion is satisfied, the experimental results depend on the surface dilatation only through the apparatus constant. This makes the data interpretation much easier. The knowledge of the apparatus constant gives a general time scale (universal surface age) that makes the results independent of the specific bubble-pressure setup and produces dynamic surface tension curves that are universal characteristics of the investigated solutions. A new equation for data processing is proposed, which provides excellent fits of the dynamic surface tension. In the case of micellar solutions, the data analysis enables one to identify the kinetic regime of adsorption (among four possible regimes). For the investigated surfactant solutions, the diffusion regime "BC" was identified, for which the fast micellar process is equilibrated, whereas the slow micellar process is negligible. Upgraded with the developed approach for quantitative data interpretation, the bubble-pressure tensiometry could be a useful tool for a detailed analysis of the adsorption processes in more complex systems.

1. Introduction

The maximum bubble pressure method (MBPM) has found wide application for characterizing the dynamics of adsorption of various surfactants. This method is especially useful in the case of fast adsorption, which is typical for surfactant concentrations around and above the critical micellization concentration (CMC). In the first works, the MBPM was applied to pure liquids.[1−3] Later, it was applied to surfactant solutions[4−10] and has been refined and adapted in many ways.[11−20] The history of this method, its development, and the limits of applicability are described in several reviews.[21−24]

The dynamics of bubble formation has been investigated by high-speed cinematography in several studies.[9,14,15,17] It was established that if the inner wall of the capillary is hydrophilic then, after the detachment of each bubble, solution enters the capillary and is further replaced by the gas flux.[9] This phenomenon leads to a more complicated and irreproducible regime of expansion of the air−water interface. For this reason, it was recommended to use capillaries with a hydrophobic inner wall and hydrophilic tip.[17] For such capillaries, the contact line solid−water−gas is fixed at the inner edge of the capillary orifice.

The quantitative interpretation of the MBPM data demands one to take into account the fact that the surfactant adsorbs at an expanding interface.[12,17,19,25−29] The cinematography of bubble growth provides direct evidence for the time dependence of the bubble surface area, $A(t)$. The latter dependence is different for apparatuses of different constructions of the gas supply system. For example, in ref 17, this system contained a reservoir and a chamber, whose volume was varied between 0.5 and 50 cm^3. For

* Corresponding author. Phone: (+359) 2-962 5310. Fax: (+359) 2-962 5438. E-mail: pk@lcpe.uni-sofia.bg.
[†] University of Sofia.
[‡] Unilever Research & Development.

(1) Simon, M. *Ann. Chim. Phys.* **1851**, *32*, 5.
(2) Schrödinger, E. *Ann. Phys.* **1915**, *46*, 413−418.
(3) Sugden, S. *J. Chem. Soc.* **1922**, *121*, 858−866; *J. Chem. Soc.* **1924**, *125*, 27−31.
(4) Rehbinder, P. A. *Z. Phys. Chem.* **1924**, *111*, 447−464.
(5) Adam, N. K.; Shute, H. L. *Trans. Faraday Soc.* **1938**, *34*, 758−765.
(6) Kuffner, R. J. *J. Colloid Sci.* **1961**, *16*, 497−500.
(7) Kragh, A. M. *Trans. Faraday Soc.* **1964**, *60*, 225−232.
(8) Austin, M.; Bright, B. B.; Simpson, E. A. *J. Colloid Interface Sci.* **1967**, *23*, 108−112.
(9) Bendure, R. L. *J. Colloid Interface Sci.* **1971**, *35*, 238−248.
(10) Kloubek, J. *J. Colloid Interface Sci.* **1972**, *41*, 17−32.
(11) Razouk, R.; Walmsley, D. *J. Colloid Interface Sci.* **1974**, *47*, 515−519.
(12) Joos, P.; Rillaerts, E. *J. Colloid Interface Sci.* **1981**, *79*, 96−100.
(13) Mysels, K. J. *Langmuir* **1986**, *2*, 428−432; *Langmuir* **1989**, *5*, 442−447.
(14) Garrett, P. R.; Ward, D. R. *J. Colloid Interface Sci.* **1989**, *132*, 475−490.
(15) Mysels, K. J. *Colloids Surf.* **1990**, *43*, 241−262.
(16) Miller, R.; Joos, P.; Fainerman, V. B. *Adv. Colloid Interface Sci.* **1994**, *49*, 249−302.
(17) Horozov, T. S.; Dushkin, C. D.; Danov, K. D.; Arnaudov, L. N.; Velev, O. D.; Mehreteab, A.; Broze, G. *Colloids Surf. A* **1996**, *113*, 117−126.
(18) Kovalchuk, V. I.; Dukhin, S. S. *Colloids Surf. A* **2001**, *192*, 131−155.
(19) Mishchuk, N. A.; Dukhin, S. S.; Fainerman, V. B.; Kovalchuk V. I.; Miller, R. *Colloids Surf. A* **2001**, *192*, 157−175.
(20) Fainerman V. B.; Kazakov V. N.; Lylyk S. V.; Makievski A. V.; Miller R. *Colloids Surf. A* **2004**, *250*, 97−102.
(21) Rusanov, A. I.; Prokhorov, V. A. *Interfacial Tensiometry*; Elsevier: Amsterdam, The Netherlands, 1996.
(22) Fainerman, V. B.; Miller, R. In *Drops and Bubbles in Interfacial Science*; Möbius, D., Miller, R., Eds.; Elsevier: Amsterdam, The Netherlands, 1998; pp 279−326.
(23) Eastoe, J.; Dalton, J. S. *Adv. Colloid Interface Sci.* **2000**, *85*, 103−144.
(24) Fainerman, V. B.; Miller, R. *Adv. Colloid Interface Sci.* **2004**, *108*−109, 287−301.
(25) Kralchevsky, P. A.; Radkov, Y. S.; Denkov, N. D. *J. Colloid Interface Sci.* **1993**, *161*, 361−365.
(26) Danov, K. D.; Vlahovska, P. M.; Horozov, T. S.; Dushkin, C. D.; Kralchevsky, P. A.; Mehreteab, A.; Broze, G. *J. Colloid Interface Sci.* **1996**, *183*, 223−235.
(27) Danov, K. D.; Kralchevsky, P. A.; Ivanov, I. B. In *Handbook of Detergents. Part. A: Properties*; Broze, G., Ed., Marcel Dekker: New York, 1999; pp 303−418.
(28) Makievski, A. V.; Fainerman, V. B.; Joos, P. *J. Colloid Interface Sci.* **1994**, *166*, 6−13.
(29) Miller, R.; Makievski, A. V.; Fainerman, V. B. In *Surfactants: Chemistry, Interfacial Properties, Applications*; Fainerman, V. B., Möbius, D., Miller, R., Eds.; Elsevier: Amsterdam, 2001; pp 287−399.

10.1021/la061239h CCC: $33.50 © 2006 American Chemical Society
Published on Web 08/03/2006

a greater chamber volume, the amplitude of pressure variations is smaller during the bubbling period, which affects the time dependence of the gas flow rate and the rate of bubble growth. The measurement of $A(t)$ in each separate experiment renders the experimental procedure difficult. Such measurements are not used in the commercially available MBPM tensiometers. However, if $A(t)$ is unknown, a quantitative data interpretation is impossible.

The key to resolve the above problem is the finding by Horozov et al.[17] that the experimental dependence $A(t_d)$ is insensitive to the bubbling period and to the surfactant type and concentration. Here, $t_d = t/t_{age}$ is the dimensionless time, with t_{age} being the nominal surface age, i.e., the time interval between the onset of bubble growth and the moment of maximum pressure. The above finding is confirmed in the present study. Here, we make the next step: It is established that, under typical experimental conditions (with a typical bubble-pressure setup, such as Krüss BP2), the experimental dynamic-surface-tension curves depend only on an integral of $A(t_d)$, called the apparatus constant, λ. For a given MBPM setup, with a given working capillary, the constant λ can be determined in experiments with a standard solution (calibration procedure), and further, the same value of λ can be used for quantitative interpretation of various data obtained with the same experimental setup. Thus, the labor consuming cinematographic determination of $A(t_d)$ is avoided. The procedures of data processing and interpretation demand an additional theoretical analysis, which is also presented below.

The paper is organized as follows. In Section 2, we consider the two main problems encountered when applying the MBPM: (i) the fact that different kinetic curves are obtained by different apparatuses for the same surfactant solution and (ii) the fact that the bubble surface is "younger" than the nominal surface age given by the MBPM apparatuses. In Section 3, we present new experimental data for the ionic surfactants sodium dodecyl sulfate (SDS) and dodecyl-trimethylammonium bromide (DTAB). Video-frames illustrating the process of bubble growth are also shown. Section 4 is devoted to a new procedure for primary data processing, which involves fits of the data and determination of three adjustable parameters, one of them being the equilibrium surface tension. In Section 5, the adsorption dynamics is modeled theoretically. Two independent ways for determining the apparatus constant are proposed and compared. Finally, in Section 6, we give interpretation of the MBPM data for concentrations above the CMC and identify which of the four possible kinetic regimes of adsorption takes place. Appendices A, B, and C, containing additional experimental data and theoretical results, are given as Supporting Information.

2. Physicochemical Background

2.1. Apparatus Function, $A(t_d)$, and Apparatus Constant, λ. The bubble pressure tensiometers (such as Krüss BP2) give the surface tension, γ, as a function of the nominal surface age, t_{age}. As mentioned above, t_{age} is defined as the period of time between the moments of minimum pressure (at bubble formation) and maximum pressure (before the bubble detachment). This definition of surface age excludes the so-called "dead time", which is the time interval beginning at the moment of maximum pressure and ending at the moment of minimum pressure (when the next bubble begins to grow).

One of the main problems with MBPM is that different experimental setups give different experimental curves $\gamma(t_{age})$. For example, as noted in ref 24, the $\gamma(t_{age})$ values obtained with the SITA tensiometer T60 are essentially lower than those measured by the Krüss tensiometer BP2, and data of both are lower than those measured with the MPT2 from Lauda and the BPA from Sinterface. Another example is given in Figure A.1 (Appendix A), where $\gamma(t_{age})$ curves obtained by two different tensiometers are compared.

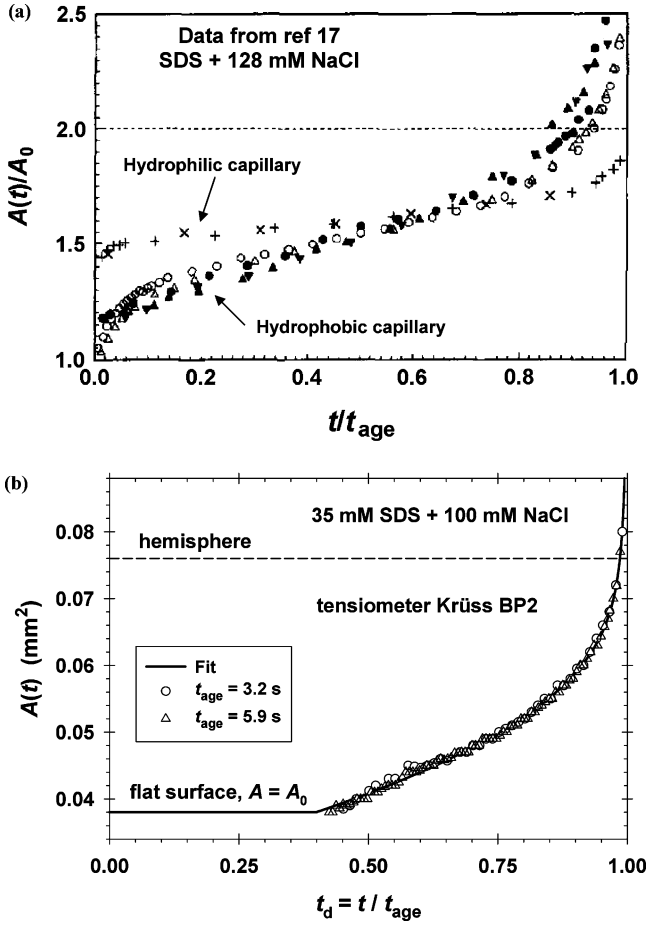

Figure 1. Time dependence of the bubble surface area $A(t)$ (the apparatus function) for two different bubble-pressure tensiometers: (a) Data from ref 17 for hydrophobic and hydrophilic capillaries at two SDS concentrations: 0.2 mM (filled symbols) and 0.4 mM; t_{age}(s) = 2.97 (+), 1.40 (×), 2.33 (●), 1.73 (▼), 1.2 (▲), 4.17 (○), and 2.27 (△). (b) New data obtained by Krüss BP2 tensiometer with silicone-oil treated capillary for t_{age} = 3.2 and 5.9 s; the solid line is fit by eq 3.1.

As already mentioned, the shape of the experimental curve, $\gamma(t_{age})$, is affected by the apparatus function, $A(t_d)$, where A is the area of the bubble surface, and $t_d = t/t_{age}$ is the dimensionless time. In general, the differences between the apparatus functions $A(t_d)$ result in different shapes of the $\gamma(t_{age})$ curves (details in Sections 3.2 and 5.3). To give a quantitative interpretation of the MBPM data, one needs to know $A(t_d)$. To determine $A(t_d)$ for a given apparatus, one has to obtain and analyze video records of the bubbling process. Experimental results are shown in Figure 1.

Figure 1a indicates that different $A(t_d)$ dependencies are obtained for two different capillaries, hydrophobic and hydrophilic, with the same tensiometer. (The use of a hydrophobic capillary is preferable; see Section 3.3.) However, the $A(t_d)$ curves in Figure 1, obtained with the same type hydrophobic capillary at different surfactant concentrations and/or bubbling periods, t_{age}, practically coincide. In other words, for the data in Figure 1, the apparatus function, $A(t_d)$, and the apparatus constant, λ, (the latter being an integral of $A(t_d)$; see eq 5.26) are independent of the surfactant type and concentration and of the bubbling period. The hypothesis that the latter result has a general validity

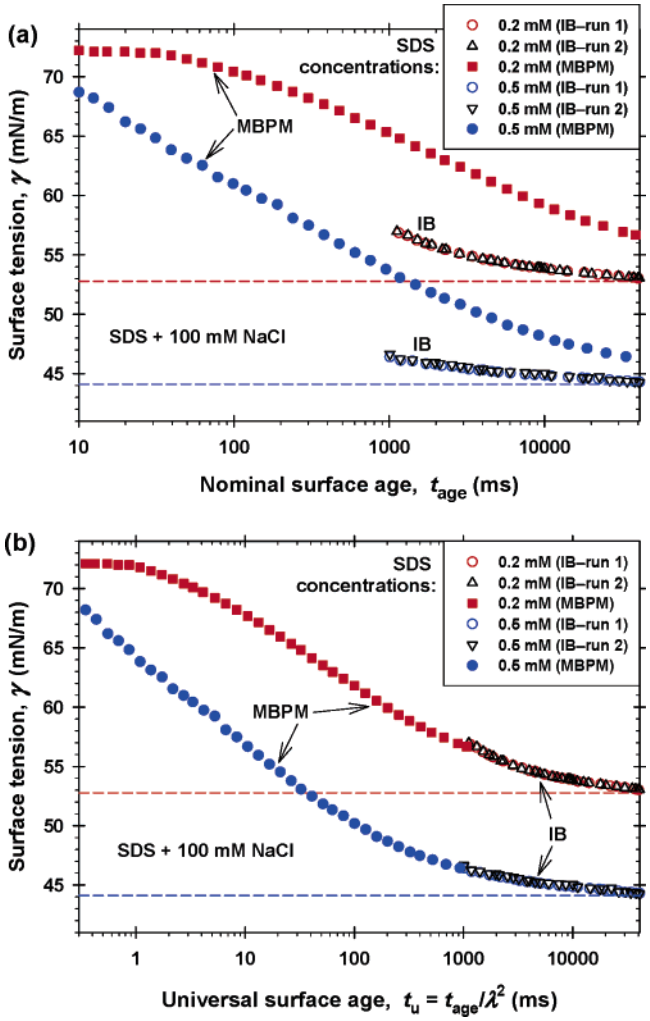

Figure 2. (a) Experimental dynamic-surface-tension curves measured by MBPM and immobile bubbles (IB) are different if the MBPM data are plotted vs the nominal surface age, t_{age}. (b) The experimental data obtained by MBPM and IB lie on the same curve if the data are plotted vs the universal surface age, $t_u = t_{age}/\lambda^2$; for our MBPM setup (expanding interface) $\lambda = 6.07$ (Section 5), while for the IB data (immobile interface) $\lambda = 1$ by definition. The horizontal dashed lines show the respective equilibrium surface tensions.

is supported by our results in Section 5.3: For all investigated solutions and bubbling periods (19 solutions of two different surfactants in the whole experimental time scale 10 ms $\leq t_{age} \leq$ 40 s), we obtain the same value of λ. In other words, it turns out that the apparatus constant, λ, characterizes the tensiometer and does not depend on the nature of the investigated solution and on the given bubbling period.

It should be also noted that it is time-consuming and inconvenient to measure experimentally the curves $A(t_d)$ by analysis of video records (as in Figure 1). For this reason, in Section 5.3, we have developed a much simpler approach. As established there, when the apparatus constant λ is sufficiently large (eq 5.29), then it is not necessary to know the apparatus function, $A(t_d)$, to interpret the experimental data. It is sufficient to determine the apparatus constant, λ, by a calibration procedure, i.e., by conventional MBPM dynamic-surface-tension measurements with a standard solution. After that, the determined λ can be used to interpret the data from all other experiments with the given tensiometer; details in Section 5.3.

2.2. Universal Surface Age. Figure 2a illustrates the fact that the actual bubble-surface age at the moment of maximum pressure (when γ is registered) is lower than the nominal surface age, t_{age}, given by the MBPM apparatus. For the same surfactant concentrations (0.2 and 0.5 mM SDS), we measured $\gamma(t)$-curves by means of the MBPM (Krüss BP2), as well as with immobile bubbles (IB). The latter were formed by means of the "EasyDrop" apparatus (Krüss) using an approach similar to that in refs 30−32. One sees (Figure 2a) that the dynamic surface tension measured by MBPM is systematically greater than that measured by IB. This fact is understandable, because for MBPM the surface is continuously expanding during the period of adsorption, whereas for the IB, the surface area is fixed. Moreover, the bubble growth is accompanied by a hydrodynamic flow and convective transport of surfactant, while such effect is missing in the case of IB. It should be also noted that the different apparatus functions, $A(t_d)$, make incomparable the nominal surface ages, t_{age}, obtained by different MBPM tensiometers.

In Section 5, we demonstrate that, when the MBPM apparatus constant, λ, is sufficiently large, then the bubble surface age at the moment of maximum pressure is equivalent by adsorption (and by surface tension) to an initially clean immobile surface of age

$$t_u \equiv t_{age}/\lambda^2 \qquad (2.1)$$

see eq 5.39. Here, as usual, t_{age} is the nominal surface age indicated by the MBPM tensiometer, whereas t_u represents a universal surface age, insofar as it is independent of the used tensiometer and of its specific apparatus function, $A(t_d)$. For this reason, the use of the plot of γ vs t_u allows one to compare experimental data obtained by a given MBPM tensiometer with analogous data obtained by other MBPM tensiometers and other methods for dynamic surface tension measurement. Because usually $\lambda^2 \gg 1$, eq 2.1 indicates that t_u could be by 1 order of magnitude smaller than t_{age}. In other words, it turns out that the MBPM is faster than indicated by the nominal surface age, t_{age}.

As an illustration, in Figure 2a, we have plotted the MBPM data as γ vs t_{age}, whereas in Figure 2b, as γ vs t_u. In panels a and b of Figure 2, the IB data are plotted in the same time scale, which is the experimental surface age. (For the IB method, there is no interfacial expansion and $\lambda \equiv 1$.) In Figure 2a, the curves are different for MBPM and IB. In contrast, in Figure 2b where the MBPM data are plotted as $\gamma(t_u)$, the experimental points obtained by means of the two methods lie on the same universal dynamic-surface-tension curve, corresponding to a given solution. In terms of the universal time scale (Figure 2b), the experimental surface age for the MBPM data is lower with a factor of $\lambda^2 \approx 37$ than the nominal surface age (Figure 2a). As seen in these figures, the lowest universal age is $t_u \approx 0.3$ ms, whereas the lowest nominal age is $t_{age} \approx 10$ ms. The factor λ^2 accounts for the fact that during the time interval $\Delta t = t_{age}$, the bubble surface area increases (Figure 1). The interfacial expansion renders the bubble surface younger in comparison with the case when the surface is immobile. The nominal surface age, t_{age}, does not account for the effect of interfacial expansion. In contrast, the universal surface age, $t_u = t_{age}/\lambda^2$, accounts for the expansion, and for this reason t_u gives the physically correct surface age (details in Section 5 below).

3. Experimental Section

3.1. Materials and Methods. The used ionic surfactants are sodium dodecyl sulfate (SDS; Acros Organics, Pittsburgh, PA) and dodecyl-trimethylammonium bromide (DTAB; Sigma Chemicals,

(30) Lin, S. Y.; McKeigue, K.; Maldarelli, C. *AIChE J.* **1990**, *36*, 1785−1795.
(31) Lin, S. Y.; Lu, T. L.; Hwang, W. B. *Langmuir* **1995**, *11*, 555−562.
(32) Lin, S. Y.; Tsau, R. Y.; Lin, L. W.; Chen, S. I. *Langmuir* **1996**, *12*, 6530−6536.

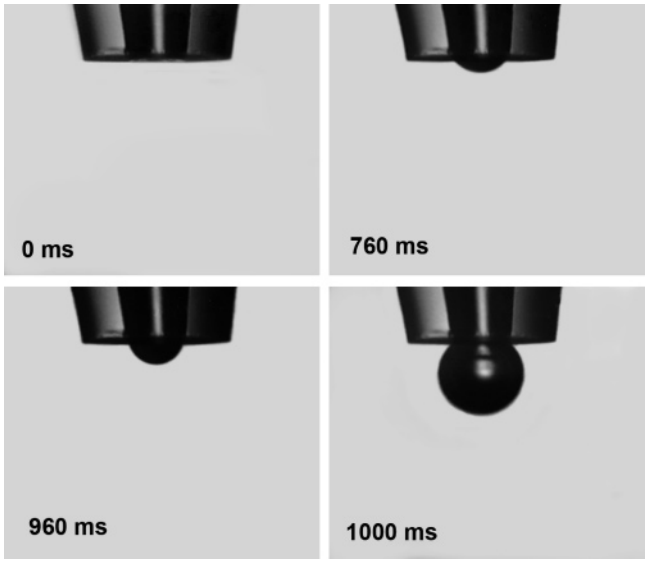

Figure 3. Consecutive photographs of a bubble growing at the tip of a capillary (inner diameter 218 μm at the orifice), which has been hydrophobized by treatment with silicone oil (see the text); $t_{age} \approx$ 1 s.

St. Louis, MO). The solutions of SDS contained 10 and 100 mM added NaCl (Merck, Darmstadt, Germany), whereas the solutions of DTAB contained 5 and 100 mM added NaBr (Merck). All solutions were prepared with pure deionized water from Millipore MilliQ system. The measurements of dynamic surface tension were performed with a processor controlled bubble pressure tensiometer Krüss BP2 (Hamburg, Germany) at temperature 27 °C. In these measurements, we used hydrophobized glass capillaries with a hydrophilic tip. The hydrophobization is necessary to ensure attachment of the growing bubbles at the inner circular edge of the capillary orifice.[17] Two hydrophobization procedures have been used.

(a) Silicone Oil Treated Capillary. First, the capillary was cleaned by sulfochromic acid, and after that, it was immersed in the mixture: H_2O_2:HCl:H_2O in ratio 1:1:5 for 30 min at 80 °C. After rinsing and drying at low temperature, it was immersed in silicone oil (48V750, Rhodia) and heated at 150 °C for 2 h. After that, it was carefully cleaned with hexane and ethanol, and finally dried.

(b) HMDS Treated Capillary. Initially, the capillary was cleaned by sulfochromic acid, then rinsed with distilled water, dried, and kept for 10 h in the atmosphere of hexamethyldisilazane (HMDS, Sigma).

Before each experiment, the capillaries of each type were rinsed with absolute ethanol and water.

3.2. Experimental Results. To investigate in detail the dynamics of bubble growth and to determine experimentally the apparatus function $A(t_d)$ (Figure 1b), we carried out direct observations of the bubbling process. For this goal, we used a specially designed optical glass cell with planar walls, instead of the original vessel of the tensiometer. The observations were carried out by means of a Zeiss stereomicroscope (Stemi 2000C) with attached black-and-white CCD video camera (Sony XC-ST50CE). To record fast moving objects, the electronic shutter of the camera was adjusted at 1/10 000 s. Digital video frames were obtained by means of TARGA$^+$ (Truevision) video capture board. Because the interval between two video frames was 40 ms, we were able to investigate in details the evolution of the bubbles at period $\geq$1 s.

Figure 3 shows illustrative photographs of the bubble evolution in a solution of 35 mM SDS + 100 mM NaCl, at the tip of a silicone-oil treated capillary of inner diameter 218 μm (at the orifice). In this case, the contact line is fixed at the tip of the capillary as the bubble grows. Quantitatively, the growth follows the curve $A(t_d)$ in Figure 1b. For $0 < t/t_{age} < 0.4$, the air−water interface is practically planar. The bubble growth occurs at $t/t_{age} \geq 0.4$, and it is strongly accelerated at $0.95 < t/t_{age} < 1$. In fact, more than 50% of the increase in the bubble area happens during the last 5% of the considered period

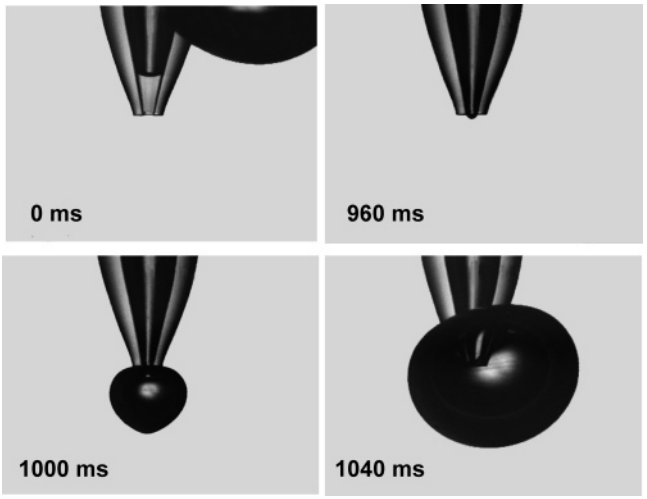

Figure 4. Consecutive photographs of a bubble growing at the tip of a capillary (inner diameter 235 μm at the orifice), which has been hydrophobized by treatment with HMDS (see the text); $t_{age} \approx$ 1 s.

(Figure 1b). The experimental dependence $\tilde{A}(t_d) \equiv A(t_d)/A_0$ can be fitted with the following empirical dependence:

$$\tilde{A}(t) = 1 \quad \text{for } t_d \equiv t/t_{age} \leq 0.4$$

$$\tilde{A}(t_d) = 0.7780 - 0.5208 \ln(1 - t_d) - 0.1020 \ln^2(1 - t_d) - 0.01151 \ln^3(1 - t_d) \quad \text{for } t_d > 0.4 \quad (3.1)$$

see the solid line in Figure 1b, where $A_0 \equiv A(0) = 0.0373$ mm^2; as usual, in eq 3.1, $t_d = t/t_{age}$ is the dimensionless time.

Figure 4 shows illustrative photographs of the evolution of a bubble at the tip of a HMDS treated capillary of inner diameter 235 μm (at the orifice). In this case, after the bubble detachment, the capillary rapidly sucks in solution (this indicates poor hydrophobization of the capillary inner wall). Then, the newly formed meniscus moves inside the capillary during the first 90% of the period t_{age}. The process of quick and spontaneous bubble expansion again takes less than 5% of the total period.

Figure A.3 (in Appendix A) shows typical dynamic-surface-tension curves, $\gamma(t_{age})$, obtained by means of the two types of capillaries, those hydrophobized by silicone oil and HMDS. In the former case, the curves are relatively smooth, while in the latter case the curves exhibit some undulations, which are probably due to the more complicated regime of bubble release. In our basic experiments (Figures 5−8), we used the capillary hydrophobized by silicone oil, which provides a regular regime of bubble formation, described by the apparatus function, $A(t_d)$, given by eq 3.1.

Experimental results obtained by means of a tensiometer Krüss BP2 for solutions of SDS and DTAB are shown in Figures 5−8 for concentrations both below and above the CMC. In each figure, the $\gamma(t_{age})$ curve corresponding to the CMC is denoted by full circles. The experimental curves are reproducible. Each experimental point in Figures 5−8 represents the average of three runs; the standard deviation is on the order of the size of the symbols. The theoretical fits are drawn by means of eq 4.5; see Section 4, where the comparison of theory and experiment is presented and discussed; for micellar solutions,[33−35] and admixture effects,[36] see Sections 6 and 4.4.

4. Primary Data Processing

4.1. Theoretical Background. For small deviations of the adsorption, Γ, from its equilibrium value, Γ_{eq}, we have

$$\Gamma = \Gamma_{eq} - s_\Gamma t^{-1/2} \quad (4.1)$$

(33) Danov, K. D.; Kralchevsky, P. A.; Denkov, N. D.; Ananthapadmanabhan, K. P.; Lips, A. *Adv. Colloid Interface Sci.* **2006**, *119*, 1−16.

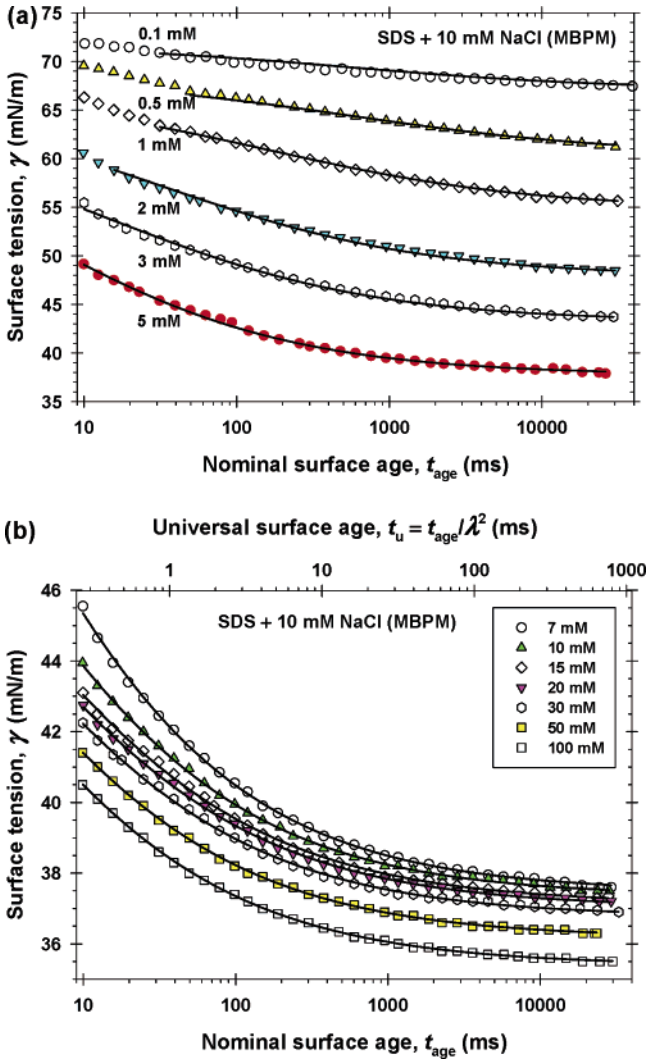

Figure 5. SDS aqueous solutions + 10 mM NaCl: Data for the dynamic surface tension, γ, vs the nominal surface age, t_{age}, measured by MBPM at SDS concentrations denoted in the figure: (a) 0.1−5 mM SDS; (b) 7−100 mM SDS. The solid lines represent the best fits by eq 4.5. The curve for 5.0 mM is close to the CMC (= 4.65 mM).

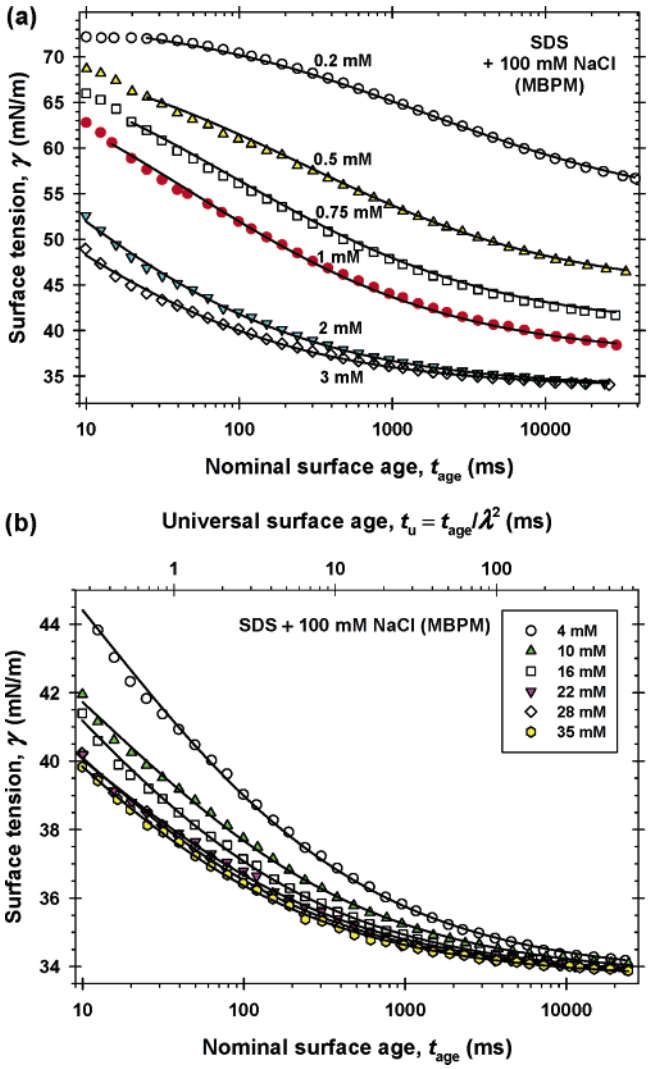

Figure 6. SDS aqueous solutions + 100 mM NaCl: Data for the dynamic surface tension, γ, vs the nominal surface age, t_{age}, measured by MBPM at SDS concentrations denoted in the figure: (a) 0.2−3 mM SDS; (b) 4−35 mM SDS. The solid lines represent the best fits by eq 4.5. The curve for 1.0 mM is close to the CMC (= 1.37 mM).

where s_Γ is the slope of the plot Γ vs $t^{-1/2}$ and, as usual, t is time. This dependence is valid for simple relaxation after an initial perturbation[29] and for the adsorption at the surface of a growing bubble (see eq 5.28). Note that, for surfactant concentrations around the CMC, the equilibrium adsorption is almost constant, $\Gamma_{eq} \approx \Gamma_{CMC}$; that is, it is insensitive to the bulk surfactant concentration. For this reason, even large perturbations in the bulk concentration produce a small effect on the adsorption, which can be therefore described by the asymptotic eq 4.1.

As a surface equation of state, connecting γ and Γ, we will use the two-dimensional van der Waals equation

$$\gamma = \gamma_0 - kT\Gamma_\infty \frac{\Gamma}{\Gamma_\infty - \Gamma} + \beta\Gamma^2 \qquad (4.2)$$

which has been found to describe very well equilibrium surface tension isotherms.[37−40] Here, k is the Boltzmann constant, T is the temperature, β is a parameter accounting for the interaction between the adsorbed surfactant molecules, Γ_∞ is the maximum possible adsorption, and γ_0 is the surface tension of the pure solvent. As usual, for diffusion-limited adsorption, we will assume that the surface equation of state (eq 4.2) can be applied to both equilibrium and dynamic processes.[41] Substituting Γ from eq 4.1 into eq 4.2, we obtain

$$\gamma = \gamma_0 - kT\Gamma_\infty \frac{\Gamma}{\Gamma_\infty - \Gamma_{eq} + s_\Gamma t^{-1/2}} + \beta\Gamma^2 \qquad (4.3)$$

As already mentioned, for surfactant concentrations around and above the CMC, the adsorption layer is densely packed, and $\Gamma_\infty - \Gamma_{eq}$ is a relatively small quantity, which could be comparable to $s_\Gamma t^{-1/2}$. For this reason, when processing experimental data

(34) Danov, K. D.; Kralchevsky, P. A.; Denkov, N. D.; Ananthapadmanabhan, K. P.; Lips, A. *Adv. Colloid Interface Sci.* **2006**, *119*, 17−33.
(35) Danov, K. D.; Kralchevsky, P. A.; Ananthapadmanabhan, K. P.; Lips, A. *Colloids Surf. A* **2006**, *282*−*283*, 143−161.
(36) Hines, J. D. *J. Colloid Interface Sci.* **1996**, *180*, 488−492.
(37) Kralchevsky, P. A.; Danov, K. D.; Kolev, V. L.; Broze, G.; Mehreteab, A. *Langmuir* **2003**, *19*, 5004−5018.
(38) Kolev, V. L.; Danov, K. D.; Kralchevsky, P. A.; Broze, G.; Mehreteab, A. *Langmuir* **2002**, *18*, 9106−9109.
(39) Valkovska, D. S.; Shearman, G. C.; Bain, C. D.; Darton, R. C.; Eastoe, J. *Langmuir* **2004**, *20*, 4436−4445.
(40) Danov, K. D.; Kralchevska, S. D.; Kralchevsky, P. A.; Ananthapadmanabhan, K. P.; Lips, A. *Langmuir* **2004**, *20*, 5445−5453.
(41) Joos, P. *Dynamic Surface Phenomena*; AH Zeist, VSP BV: The Netherlands, 1999.

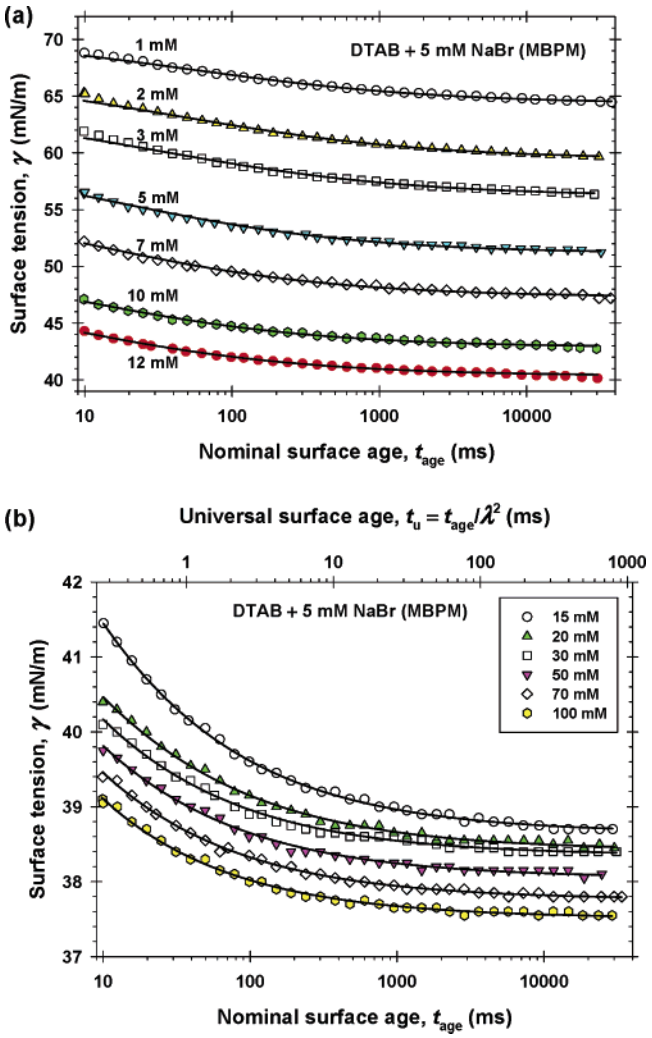

Figure 7. DTAB aqueous solutions + 5 mM NaBr: Data for the dynamic surface tension, γ, vs the nominal surface age, t_{age}, measured by MBPM at DTAB concentrations denoted in the figure: (a) 1−12 mM DTAB; (b) 15−100 mM DTAB. The solid lines represent the best fits by eq 4.5. The curve for 12 mM is close to the CMC (= 13.4 mM).

(like those in Figures 5−8), we will not expand the denominator of eq 4.3 in series for small $t^{-1/2}$. Instead, in eq 4.2, we substitute $\Gamma = \Gamma_{eq}$ and $\gamma = \gamma_{eq}$ and subtract the result from eq 4.3; thus, we derive

$$\gamma = \gamma_{eq} - \frac{kT\Gamma_\infty^{\,2}}{\Gamma_\infty - \Gamma_{eq}} \frac{\Gamma - \Gamma_{eq}}{\Gamma_\infty - \Gamma} \times \left[1 - \frac{\beta}{kT\Gamma_\infty^{\,2}}(\Gamma + \Gamma_{eq})(\Gamma_\infty - \Gamma_{eq})(\Gamma_\infty - \Gamma)\right] \quad (4.4)$$

Finally, we substitute Γ from eq 4.1 into eq 4.4, and where possible we neglect $s_\Gamma t^{-1/2}$ in comparison with Γ_{eq}. As a result, we obtain

$$\gamma = \gamma_{eq} + \frac{s_\gamma}{a_\gamma + t_{age}^{\,1/2}} \quad (4.5)$$

where $t \equiv t_{age}$ and the parameters s_γ and a_γ are

$$s_\gamma = kTs_\Gamma\left[\frac{\Gamma_\infty^{\,2}}{(\Gamma_\infty - \Gamma_{eq})^2} - \frac{2\beta\Gamma_{eq}}{kT}\right] \quad (4.6)$$

$$a_\gamma = \frac{s_\Gamma}{\Gamma_\infty - \Gamma_{eq}} \quad (4.7)$$

The asymptotic eq 4.5 is valid for not-too-small values of t_{age} (for not-too-low surface coverage). Note that for long times eq 4.5 reduces to the known asymptotics $\gamma = \gamma_{eq} + s_\gamma t_{age}^{-1/2}$, where s_γ is the slope of the plot of γ vs $t_{age}^{-1/2}$. In applications, sometimes it is convenient to represent eq 4.5 in the equivalent form of a three-parameter rational function of $t_{age}^{1/2}$

$$\gamma(t) \approx \frac{b_\gamma + \gamma_{eq} t_{age}^{\,1/2}}{a_\gamma + t_{age}^{\,1/2}} \quad (b_\gamma \equiv s_\gamma + a_\gamma\gamma_{eq}) \quad (4.8)$$

The experimental data for $\gamma(t_{age})$ are to be fitted by means of eq 4.5 or 4.8. The parameters γ_{eq}, a_γ, and s_γ in eq 4.5 (or γ_{eq}, a_γ, and b_γ in eq 4.8) are to be determined from the best fit.

4.2. Results from the Fits of the Data. The experimental curves in Figures 5−8 can be fitted by either eq 4.5, or its equivalent form, eq 4.8. In Figures 5a, 6a, 7a, and 8a, the theoretical curves are drawn in the region of not-too-short t_{age}, where eq 4.5 is applicable. One sees that only some points in the left-upper corner of these plots do not comply with eq 4.5. On the other hand, in Figures 5b, 6b, 7b, and 8b, eq 4.5 is applicable in the whole experimental time-span from 10 ms to 30 s.

The nonlinear data fit with eq 4.5 is more general than the fit with the asymptotic linear dependence $\gamma = \gamma_{eq} + s_\gamma t_{age}^{-1/2}$, which is valid only for sufficiently long times. To illustrate that, in Figure 9, we have plotted four of the curves in Figure 8 (both theoretical curves and experimental points) as γ vs $t_{age}^{-1/2}$. One sees that the theoretical fits by eq 4.5 describe very well the experimental data in the whole region, including the asymptotic linear region at $t_{age}^{-1/2} \to 0$. Hence, the fit by eq 4.5 removes the uncertainty about the drawing of the linear asymptotic fit γ vs $t_{age}^{-1/2}$, as discussed in Appendix A (Figure A.2). This uncertainty is related to a possible inaccurate determination of the slope of the asymptotic (at $t_{age}^{-1/2} \to 0$) tangent to the experimental curves, like those in Figure 9.

The parameters γ_{eq}, s_γ, and a_γ, determined from the best fits of the data for SDS in Figures 5 and 6, are listed in Table 1, whereas in the case of DTAB, the parameter values from the fits in Figures 7 and 8 are given in Table 2. The regression coefficient, R, which is also listed in these tables, is a measure of how well the regression curve describes the data ($0 < R < 1$). R values near 1, as those in Tables 1 and 2, indicate that the respective theoretical curves agree very well with the experimental data. From the values of s_γ, one can determine the apparatus constant, λ (see Section 5.3). In the next subsection, we demonstrate that the values of the equilibrium surface tension, γ_{eq}, obtained by means of MBPM (Tables 1 and 2), agree well with the independently determined values of γ_{eq}.

4.3. Equilibrium Surface Tension of SDS and DTAB Determined by MBPM. The symbols in Figure 10 show the values of γ_{eq} for SDS and DTAB determined by MBPM (Tables 1 and 2). The kink in each curve corresponds to the CMC. The obtained parameter values at the CMC compare very well with values determined by other authors. For example, for SDS + 100 mM NaCl, the determined values of CMC = 1.37 mM and $\Gamma_{CMC} = 4.1 \times 10^{-6}$ mol/m^2 are close to the values CMC = 1.62 mM and $\Gamma_{CMC} = 4.3 \times 10^{-6}$ mol/m^2 obtained by Tajima[42] for SDS solutions with 115 mM NaCl. (The above values of Γ_{CMC} were calculated by substituting $c_{1\infty}$ = CMC in the system of eqs

(42) Tajima, K. *Bull. Chem. Soc. Jpn.* **1970**, *43*, 3063−3066.

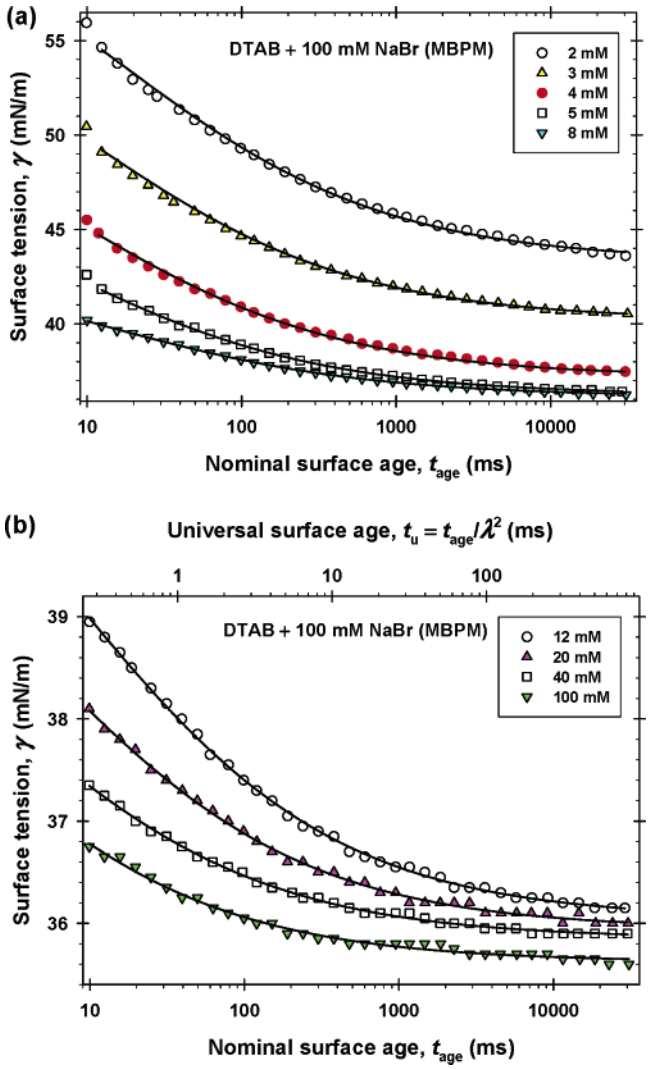

Figure 8. DTAB aqueous solutions + 100 mM NaBr: Data for the dynamic surface tension, γ, vs the nominal surface age, t_{age}, measured by MBPM at DTAB concentrations denoted in the figure: (a) 2−8 mM DTAB; (b) 12−100 mM DTAB. The solid lines represent the best fits by eq 4.5. The curve for 4 mM is close to the CMC (= 4.25 mM).

4.9−4.11, using the parameter values in Table 3; the solution of the latter system gives $\Gamma_1 = \Gamma_{CMC}$; see below.) For DTAB + 100 mM NaBr, the determined values of CMC = 4.25 mM and γ_{CMC} = 35.6 mN/m are very close to the values CMC = 4.4 mM and γ_{CMC} = 36.2 mN/m reported, respectively, in refs 43 and 44 for the same system.

For concentrations below the CMC, there are accurate theoretical models, whose parameters can be determined by fitting simultaneously a set of equilibrium surface tension isotherms of ionic surfactants corresponding to different electrolyte concentrations. After that, the model allows one to calculate (predict) the surface tension (as well as the surfactant adsorption, counterion binding, surface electric potential, surface elasticity, etc.) for every given couple of surfactant and salt concentrations.[37−40] To draw the continuous lines in Figures 10 and 11 for concentrations below the CMC, we used a van der Waals type of model,[45] which has been applied[38,39] to fit respectively data for SDS and DTAB.

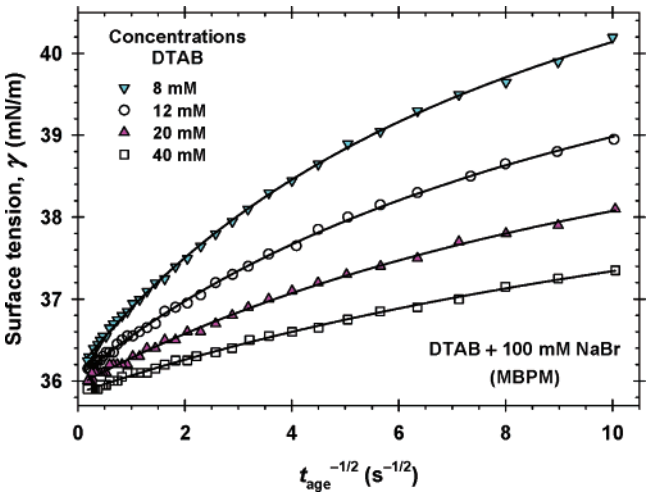

Figure 9. Plot of MBPM data for γ vs $t_{age}^{-1/2}$ from Figure 8. The solid lines are fits by means of eq 4.5. The theoretical curves are essentially nonlinear, but asymptotically yield the linear dependence $\gamma = \gamma_{eq} + s_\gamma\, t_{age}^{-1/2}$, as guarantied by eq 4.5.

Table 1. Parameters for SDS from the Fits of the Data in Figures 5 and 6 by eq 4.5

C_{SDS} (mM)	γ_{eq} (mN/m)	s_γ (mN·s$^{1/2}$·m^{-1})	a_γ (s$^{1/2}$)	R
		10 mM NaCl		
0.1	67.12 ± 0.07	3.36 ± 0.3	0.734 ± 0.09	0.9940
0.5	60.46 ± 0.05	5.95 ± 0.2	0.760 ± 0.03	0.9991
1	54.84 ± 0.05	4.83 ± 0.2	0.399 ± 0.02	0.9994
2	47.90 ± 0.09	3.31 ± 0.2	0.177 ± 0.02	0.9982
3	43.25 ± 0.09	2.57 ± 0.2	0.123 ± 0.02	0.9979
5[a]	37.74 ± 0.08	1.84 ± 0.1	0.062 ± 0.02	0.9977
7	37.47 ± 0.02	1.06 ± 0.02	0.034 ± 0.002	0.9996
10	37.35 ± 0.02	0.926 ± 0.01	0.042 ± 0.002	0.9997
15	37.13 ± 0.02	0.878 ± 0.02	0.049 ± 0.003	0.9994
20	37.03 ± 0.02	0.842 ± 0.02	0.049 ± 0.003	0.9996
30	36.77 ± 0.02	0.796 ± 0.02	0.046 ± 0.003	0.9995
50	36.17 ± 0.01	0.733 ± 0.01	0.040 ± 0.003	0.9989
100	35.39 ± 0.02	0.688 ± 0.02	0.035 ± 0.003	0.9970
		100 mM NaCl		
0.2	53.10 ± 0.05	27.7 ± 0.3	1.30 ± 0.02	0.9999
0.5	44.37 ± 0.07	14.0 ± 0.2	0.507 ± 0.01	0.9999
0.75	40.22 ± 0.08	10.1 ± 0.2	0.306 ± 0.007	0.9997
1[a]	37.19 ± 0.06	7.89 ± 0.1	0.218 ± 0.006	0.9998
2	33.76 ± 0.07	3.11 ± 0.08	0.071 ± 0.005	0.9992
3	33.75 ± 0.07	2.37 ± 0.07	0.064 ± 0.005	0.9990
4	33.74 ± 0.06	2.23 ± 0.07	0.109 ± 0.007	0.9989
10	33.71 ± 0.04	1.69 ± 0.04	0.112 ± 0.005	0.9993
16	33.69 ± 0.03	1.33 ± 0.03	0.078 ± 0.005	0.9993
22	33.67 ± 0.03	1.23 ± 0.03	0.092 ± 0.005	0.9992
28	33.66 ± 0.03	1.11 ± 0.03	0.073 ± 0.004	0.9993
35	33.66 ± 0.02	1.04 ± 0.02	0.068 ± 0.003	0.9996

[a] Concentration ≈ CMC.

The parameters of the model, determined from the best fits of the data in Figure 11, panels a and b, are given in Table 3.

In Figure 11a, we compare the values of γ_{eq} obtained from the MBPM data (Table 1 and Figure 10a) with available data[46] for γ_{eq} measured by means of the drop-shape analysis (DSA) method for the same sample of SDS (Acros). Both sets of experimental results contain data at 10 mM NaCl, for which excellent agreement is observed (Figure 11a). The γ_{eq} data for the three NaCl concentrations are fitted simultaneously by means of the van der Waals type model[38,45] by using only four adjustable parameters, whose values (corresponding to the best fit) are given in Table 3.

In Figure 11b, we compare the values of γ_{eq} determined by MBPM (Table 2 and Figure 10b) with available data for γ_{eq}

(43) Emerson, M. F.; Holtzer, A. *J. Phys. Chem.* **1967**, *71*, 1898−1907.
(44) Henderson, D. C.; Micale, F. J. *J. Colloid Interface Sci.* **1993**, *158*, 289−294.
(45) Kralchevsky, P. A.; Danov K. D.; Broze G.; Mehreteab, A. *Langmuir* **1999**, *15*, 2351−2365.

Table 2. Parameters for DTAB from the Fits of the Data in Figures 7 and 8 by eq 4.5

C_{SDS} (mM)	γ_{eq} (mN/m)	s_γ (mN·s$^{1/2}$·m^{-1})	a_γ (s$^{1/2}$)	R
		5 mM NaBr		
1	64.34 ± 0.03	1.35 ± 0.05	0.218 ± 0.01	0.9985
2	59.50 ± 0.02	1.43 ± 0.04	0.175 ± 0.01	0.9992
3	56.24 ± 0.03	1.32 ± 0.04	0.155 ± 0.01	0.9988
5	51.15 ± 0.03	1.08 ± 0.04	0.113 ± 0.009	0.9994
7	47.31 ± 0.04	0.912 ± 0.06	0.093 ± 0.008	0.9995
10	42.86 ± 0.04	0.738 ± 0.04	0.083 ± 0.01	0.9987
12[a]	40.35 ± 0.02	0.657 ± 0.02	0.073 ± 0.004	0.9990
15	38.65 ± 0.01	0.316 ± 0.01	0.013 ± 0.003	0.9994
20	43.33 ± 0.01	0.245 ± 0.01	0.020 ± 0.005	0.9980
30	38.42 ± 0.01	0.198 ± 0.008	0.009 ± 0.005	0.9980
50	38.35 ± 0.01	0.196 ± 0.009	0.011 ± 0.005	0.9974
70	38.05 ± 0.01	0.183 ± 0.006	0.008 ± 0.004	0.9986
100	37.76 ± 0.01	0.162 ± 0.006	0.002 ± 0.004	0.9979
		100 mM NaBr		
2	43.13 ± 0.04	2.66 ± 0.06	0.126 ± 0.006	0.9996
3	39.55 ± 0.03	1.89 ± 0.04	0.098 ± 0.006	0.9995
4[a]	36.92 ± 0.04	1.48 ± 0.05	0.088 ± 0.007	0.9988
5	36.24 ± 0.02	1.02 ± 0.02	0.073 ± 0.003	0.9997
8	36.15 ± 0.01	0.82 ± 0.01	0.106 ± 0.004	0.9997
12	36.05 ± 0.01	0.54 ± 0.01	0.085 ± 0.004	0.9996
20	35.95 ± 0.01	0.36 ± 0.01	0.068 ± 0.006	0.9988
40	35.85 ± 0.01	0.225 ± 0.006	0.051 ± 0.005	0.9990
100	35.62 ± 0.01	0.152 ± 0.009	0.032 ± 0.009	0.9954

[a] Concentration ≈ CMC.

obtained[47] by means of the Du Noüy ring method for DTAB. The two sets of experimental results, which contain data for four different concentrations of NaBr, are consistent insofar as they can be simultaneously fitted by means of the van der Waals model, by variation of four adjustable parameters; see Figure 11b and Table 3.

Knowing the parameter values in Table 3, one can calculate the surfactant adsorption, Γ_1, the counterion adsorption, Γ_2, and the dimensionless surface electric potential, Φ_s, by numerical solution of the following system of three equations:[45]

$$K_1 a_{1\infty} \exp(-\Phi_s) = \frac{\Gamma_1 - \Gamma_2}{\Gamma_\infty - \Gamma_1} \exp\left(\frac{\Gamma_1}{\Gamma_\infty - \Gamma_1} - \frac{2\beta\Gamma_1}{kT}\right) \quad (4.9)$$

$$K_{St} a_{2\infty} \exp(\Phi_s) = \frac{\Gamma_2}{\Gamma_1 - \Gamma_2} \quad (4.10)$$

$$\Gamma_1 - \Gamma_2 = \frac{4}{\kappa_c}\sqrt{a_{2\infty}}\sinh\left(\frac{\Phi_s}{2}\right) \quad (4.11)$$

Here, $a_{1\infty} = \gamma_\pm c_{1\infty}$ and $a_{2\infty} = \gamma_\pm c_{2\infty}$ are the activities of the surfactant ions and counterions, $c_{1\infty}$ and $c_{2\infty}$ are the respective bulk concentrations, and $\gamma_\pm$ is the activity coefficient (see eq 4.12). Equations 4.9 and 4.10 are respectively the adsorption equations for surfactant at the interface and of counterions at the Stern layer; K_1 and K_{St} are the respective adsorption constants. Equation 4.11 is a form of the known Gouy[48] equation, connecting the surface charge and potential, where $\kappa_c \equiv 8\pi e^2/(\epsilon kT)$; ϵ is the dielectric constant of the solvent (water). It has been proven[45] that the integration of the Gibbs adsorption equation, $d\pi_a = kT\Sigma_i \Gamma_i\, d \ln a_{is}$, along with eqs 4.9 and 4.10 gives the van der Waals equation of state, $(\pi_a + \beta\Gamma_1^2)(1 - \Gamma_1/\Gamma_\infty) = \Gamma_1 kT$, for the surface pressure, π_a, where $a_{1s} = a_{1\infty}\exp(-\Phi_s)$ and $a_{2s} = a_{2\infty}\exp(\Phi_s)$ are the subsurface activities of the surfactant ions and counterions. The total adsorption parameter is[45] $K = K_1(1 + K_{St}a_{2s})$.

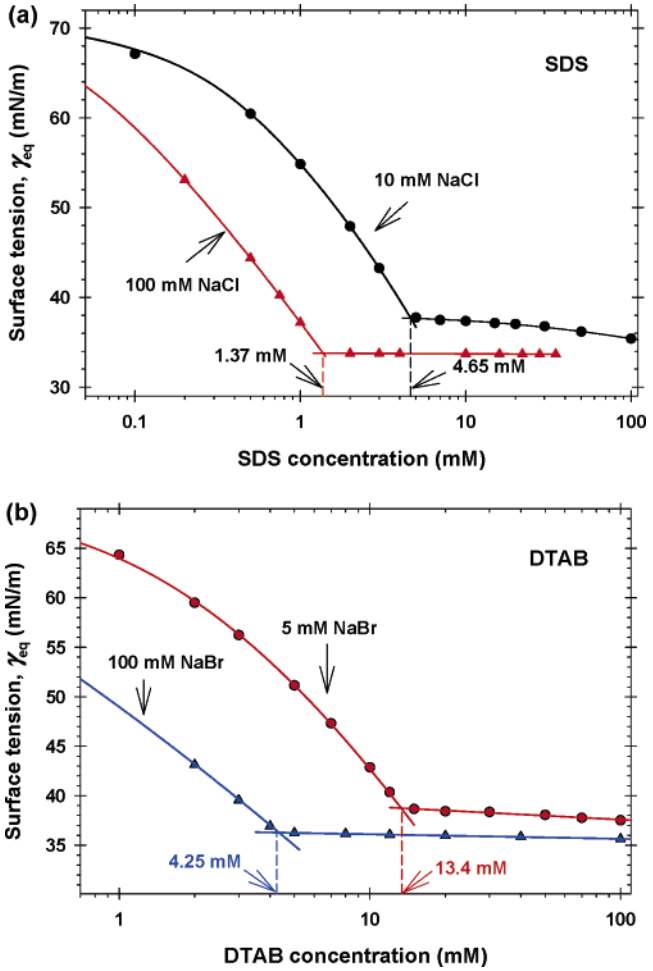

Figure 10. Plots of γ_{eq} vs the surfactant concentration: (a) Data for SDS from Table 1 and (b) Data for DTAB from Table 2. The lines for the concentrations below the CMC are fits drawn as explained in the text; see also Figure 11.

Table 3. Parameters of the van der Waals Model Determined from the Fits in Figure 11

surfactant	K_1 (mM)$^{-1}$	K_{St} (mM)$^{-1}$	Γ_∞^{-1} (Å^2)	$2\beta\Gamma_\infty/(kT)$
SDS	100.1	6.529×10^{-4}	30.0	3.56
DTAB	59.15	7.480×10^{-4}	36.5	2.69

For the values of K_1, K_{St}, Γ_∞, and β in Table 3, and for given $a_{1\infty}$ and $a_{2\infty}$, we solve the system of eqs 4.9−4.11 as follows. With a tentative value of Φ_s, from eq 4.11 one calculates $\Gamma_1 - \Gamma_2$. Next, from eq 4.10, one determines Γ_2. The results are further substituted in eq 4.9, which is solved numerically to determine Φ_s; we used the bisection method.

The activity coefficient, $\gamma_\pm$, can be calculated from the known semiempirical formula[49]

$$\log \gamma_\pm = -\frac{A\sqrt{I}}{1 + Bd_i\sqrt{I}} + bI \quad (4.12)$$

originating from the Debye−Hückel theory; I is the ionic strength of the solution; the logarithm in eq 4.12 is decimal; d_i is the diameter of the ion; A, B, and b are parameters, which are

(46) Gurkov, T. D.; Todorova, D. T.; Marinova, K. G.; Bilke-Crause, C.; Gerber, C.; Ivanov, I. B. *Colloids Surf. A* **2005**, *261*, 29−38.
(47) Battal, T.; Shearman, G. C.; Valkovska, D.; Bain, C. D.; Darton, R. C.; Eastoe, J. *Langmuir* **2003**, *19*, 1244−1248.
(48) Gouy, G. *J. Phys. Radium* **1910**, *9*, 457−468.
(49) Robinson, R. A.; Stokes, R. H. *Electrolyte Solutions*, 2nd ed.; Dover Publications: New York, 2002.

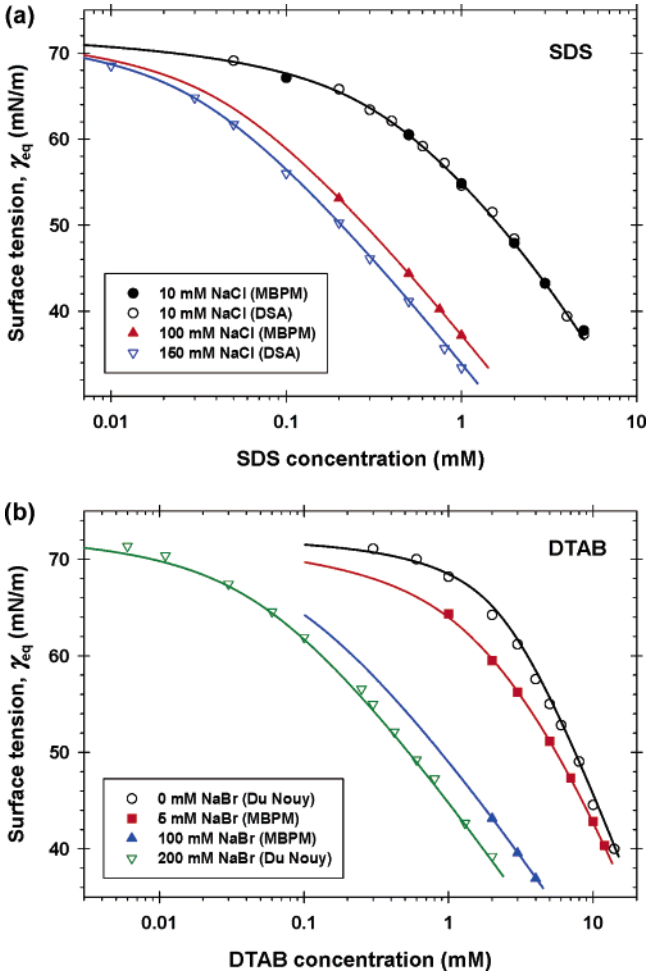

Figure 11. Plot of the equilibrium surface tension, γ_{eq}, vs the surfactant concentration. (a) SDS solutions: MBPM data from Table 1 and DSA data from ref 46. (b) DTAB solutions: MBPM data from Table 2 and data measured by the Du Nouy ring method.[47] The solid lines represent the best fit of the data for each surfactant by means of the van der Waals model.[38,45] The data for all salt concentrations are fitted simultaneously; the parameters of the model, determined from the best fit, are listed in Table 3.

tabulated;[49] for our experimental conditions, we used the values $A = 0.5115\ \mathrm{M}^{-1/2}$, $Bd_i = 1.316\ \mathrm{M}^{-1/2}$, and $b = 0.055\ \mathrm{M}^{-1}$.

The equilibrium surfactant adsorption, $\Gamma_{eq} = \Gamma_1$, determined by solving eqs 4.9−4.11 with parameter values from Table 3, will be essentially used to determine the apparatus constant in Section 5.3 below.

4.4. Effect of Nonionic Admixtures. At low ionic strengths, even trace amounts of nonionic surfactant admixtures could affect the surface tension of the ionic surfactant solutions. For example, the SDS samples often contain small admixtures of dodecanol.[36,37] At low ionic strengths, the high surface potential repels the DS^- ions from the subsurface layer and makes their subsurface concentration comparable to that of the nonionic admixture. The adsorption of the latter leads to a lower equilibrium surface tension, γ_{eq}, in comparison with that of the solution of pure SDS.

Under dynamic conditions, the effect of a nonionic admixture on γ appears at the late stages of the adsorption process. This is due to the low concentration of the admixture, which leads to its slow diffusion. An example is given in Figure 12 for SDS solutions without added NaCl. The presence of nonionic admixture leads to deviations from eq 4.5 at the long times. Excluding the data for the long times (for $t_{age}^{1/2} > 2s^{1/2}$ in Figure 12), the rest of the MBPM experimental points can be excellently

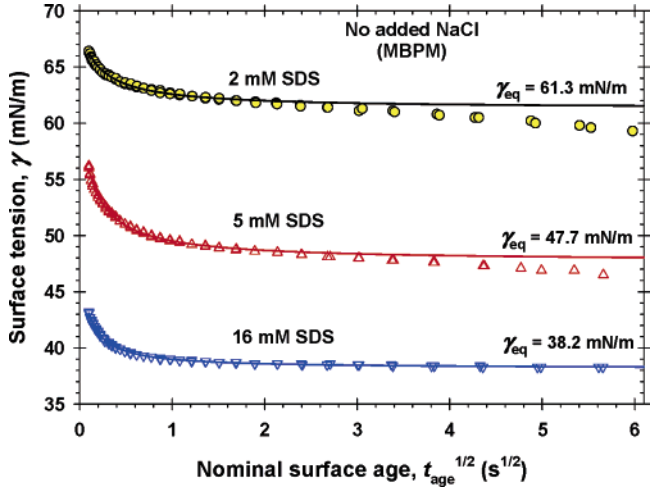

Figure 12. Solutions without added NaCl: Plot of the dynamic surface tension, γ, vs. $t_{age}^{1/2}$ for three concentrations of SDS denoted in the figure. The solid lines represent fits of the data for $t_{age}^{1/2} < 2\ s^{1/2}$ by means of eq 4.5; the values of γ_{eq} given in the figure are determined from these fits.

fitted by means of eq 4.5. Moreover, the values of the equilibrium surface tension determined from these fits, $\gamma_{eq} = 61.3$ and 47.7 mN/m, agree very well with the respective equilibrium data,[38] $\gamma_{eq} = 61.7$ and 47.8 mN/m, for pure SDS at concentrations 2 and 5 mM. At 16 mM SDS, the ionic strength of the solution (due to SDS alone) is sufficiently high to suppress the effect of the nonionic admixture (Figure 12).

In summary, the maximum bubble pressure method is sensitive to the presence of nonionic amphiphilic admixtures, which cause deviations from the fit with eq 4.5 at the long times (Figure 12). Consequently, the MBPM could be employed to quantify the amount of these admixtures. Their effect on the dynamic surface tension could be suppressed by addition of a sufficient amount of inorganic electrolyte, as in our basic experiments: 10 and 100 mM NaCl (Figures 5 and 6) and 5 and 100 mM NaBr (Figures 7 and 8). In the absence of added inorganic electrolyte, the effect of the admixtures could be avoided by exclusion of the experimental points at the long times when fitting the data by means of eq 4.5 (Figure 12).

4.5. Application of the Langmuir−Frumkin Isotherm. Instead of using the van der Waals equation of state, eq 4.2, one could try to fit the MBPM data in Figures 5−8 by means of the Frumkin equation of state[45,50]

$$\gamma = \gamma_0 + kT\Gamma_\infty \ln\left(1 - \frac{\Gamma}{\Gamma_\infty}\right) + \beta\Gamma^2 \qquad (4.13)$$

With the help of eq 4.1, from eq 4.13, we derive a counterpart of eq 4.5

$$\gamma \approx \gamma_{eq} + kT\Gamma_\infty \ln(1 + a_\gamma t_{age}^{-1/2}) + b_F t_{age}^{-1/2} \qquad (4.14)$$

a_γ is given again by eq 4.7, whereas $b_F = -2\beta\Gamma_{eq}s\Gamma$. The comparison of eq 4.14 with our experimental data (Figures 5−8), which correspond to the concentration region around the CMC, shows that in this region the term with b_F is negligible and, consequently, b_F cannot be determined from the data fits. If the last term (with b_F) in eq 4.14 is neglected, we obtain an expression corresponding to the Langmuir adsorption model

$$\gamma \approx \gamma_{eq} + kT\Gamma_\infty \ln(1 + a_\gamma t_{age}^{-1/2}) \qquad (4.15)$$

We fitted the data in Figures 5−8 with the help of eq 4.15 using

Table 4. Parameters for DTAB + 100 MM NaBr from Fits of Data in Figure 8 by eq 4.15

DTAB (mM)	γ_{eq} (mN/m)	$kT\Gamma_\infty$ (mN/m)	a_γ ($s^{1/2}$)	R
8	36.1 ± 0.3	2.83 ± 0.07	0.32 ± 0.02	0.9997
12	36.0 ± 0.4	2.5 ± 0.1	0.23 ± 0.02	0.9995
20	35.9 ± 0.7	2.1 ± 0.1	0.18 ± 0.02	0.9987
40	35.9 ± 0.8	1.8 ± 0.1	0.13 ± 0.01	0.9990

three adjustable parameters: γ_{eq}, a_γ, and Γ_∞. (We recall that the fit by means of the van der Waals model also contains three adjustable parameters: γ_{eq}, a_γ, and s_γ; see eq 4.5.) For a given solution, the fit with eq 4.15 agrees very well with the experimental data, just as the fits with the van der Waals model. The values of γ_{eq} obtained in this way are close to the values determined by means of the van der Waals model. However, it turns out that the values of the parameter Γ_∞ obtained from the fits with eq 4.15 depend on the surfactant concentration. An illustrative example is given in Table 4 for several solutions of DTAB + 100 mM NaBr.

Note that the variation of $kT\Gamma_\infty$ in Table 4 is much greater than the experimental error of the surface tension as determined from the fit. The decrease of Γ_∞ with the rise of DTAB concentration contradicts the definition of Γ_∞ as the maximum possible adsorption of DTAB. In particular, the value $kT\Gamma_\infty = 1.82$ mN/m (the last row in Table 4) corresponds to $\Gamma_\infty^{-1} = 225$ Å^2 per adsorbed molecule, which is much greater than the excluded area per DTAB molecule, the latter being ≈37 Å^2 from molecular-size considerations. The value $\Gamma_\infty^{-1} = 225$ Å^2 per molecule cannot represent the maximum possible adsorption at close packing.

In conclusion, the fit of the dynamic surface tension data by means of the Frumkin model, eq 4.15, leads to a contradiction: the concentration dependence of Γ_∞ and its nonrealistic values. In the case of the van der Waals model, instead of the geometric parameter Γ_∞, from the fit of the dynamic-surface-tension data, we determine the dynamic parameter, s_γ. The variation of s_γ with the surfactant concentration turns out to be reasonable (as demonstrated in Section 5.3, the ratio $s_\gamma/s_{\gamma,0} = \lambda$ is constant for all concentrations of the two surfactants and salts). Thus, when applying the van der Waals model, we did not face the difficulty that was encountered when applying the Frumkin model. For this reason, everywhere in this paper (except the present subsection), we use the van der Waals model.

The reason for the fact that in the considered case the van der Waals model works better than the Frumkin model could be related to the circumstance that they describe nonlocalized and localized adsorption, respectively.[51] The localized adsorption is typical for solid surfaces. In contrast, the surfactant adsorption at fluid interfaces is nonlocalized, which makes the van der Waals model more adequate for such systems.

5. Theoretical Modeling of Adsorption Dynamics

5.1. Diffusion Problem. The surfactant transport toward the surface of an expanding bubble can be described by means of the equation of convective diffusion[41]

$$\frac{\partial c}{\partial t} - \dot{\alpha} x \frac{\partial c}{\partial x} = D\frac{\partial^2 c}{\partial x^2} \tag{5.1}$$

($t > 0$ and $x > 0$). Here, t is time; c is the concentration of the surfactant molecules; x is the coordinate normal to the interface (the latter being situated at $x = 0$); D is diffusivity; $\dot{\alpha}$ is the surface dilatation rate

$$\dot{\alpha} \equiv \frac{1}{A}\frac{dA}{dt} \tag{5.2}$$

As usual, $A(t)$ is the area of the bubble surface. The convective term (that with $\dot{\alpha}$ in eq 5.1) is expressed by using the approximation by van Voorst Vader et al.[41,52] In the case of bubbles (MBPM), the use of the convective diffusion equation for planar interfaces, eq 5.1, is an approximation, which is applicable insofar as the radii of curvature of the expanding surface are much larger than the thickness of the interfacial region, so that the interface can be regarded as "locally planar".[41]

In eq 5.1, D is the diffusion coefficient, whose meaning depends on the type of the used solution, as follows:

(1) Below the CMC, for solutions of a nonionic surfactant, or of an ionic surfactant at high concentrations of added inorganic electrolyte ($c_{2\infty} \gg c_{1\infty}$), $D = D_1$ is the diffusivity of the surfactant molecules/ions. This case corresponds to the investigated solutions of SDS and DTAB + 100 mM added electrolyte (Figures 6 and 8).

(2) Above the CMC, D has the meaning of an effective diffusivity of the surfactant solution, which is greater than the monomer diffusivity, D_1.[41] Details could be found in Section 6, where it is established that the dynamic-surface-tension curves in Figures 6 and 8, for concentrations above the CMC, correspond to the so-called diffusion regime BC;[34,35] for details, see the beginning of Section 6.

(3) The general case of an ionic surfactant with or without added inorganic electrolyte, below the CMC, includes our experiments with SDS + 10 mM NaCl and DTAB + 5 mM NaBr (Figures 5 and 7). The respective theory was developed in ref 53; the results, which will be used here, are summarized below; see eqs 5.36 and 5.38, and Appendix B.

Here, we will consider the first of the above three cases: a nonionic surfactant (or an ionic surfactant at high salt concentrations), below the CMC. The initial and boundary conditions for eq 5.1 are

$$c = c_\infty \quad \text{at } t = 0 \text{ and } x > 0 \tag{5.3}$$

$$c = c_\infty \quad \text{at } t > 0 \text{ and } x \to \infty \tag{5.4}$$

where c_∞ is the bulk surfactant concentration in the investigated solution. The other boundary condition, viz. the surfactant mass balance at the interface, is affected by the surface expansion[27,41]

$$\frac{d\Gamma}{dt} + \dot{\alpha}\Gamma = D\frac{\partial c}{\partial x} \quad \text{at } t > 0 \text{ and } x = 0 \tag{5.5}$$

In eq 5.5, we have assumed that the bubble surface is uniform owing to the Marangoni effect, which suppresses the adsorption gradients. In such a case, there is no surface diffusion. It is important to note that the considered convective-diffusion problem can be reduced to a standard diffusion problem. For this goal, we replace the variables (x,t) with a new couple of variables, (y,τ), defined as follows:[27]

$$y \equiv \tilde{A}(t_d)x \quad \text{and} \quad \tau \equiv \int_0^{t_d} [\tilde{A}(\hat{t}_d)]^2 d\hat{t}_d \tag{5.6}$$

Here $\hat{t}_d$ is an integration variable; $\tilde{A}$ and t_d are the dimensionless

(50) Frumkin, A. N. *Z. Phys. Chem. (Leipzig)* **1925**, *116*, 466−484.
(51) Hill, T. L., *An Introduction to Statistical Thermodynamics*, Addison-Wesley: Reading, MA, 1962.
(52) Van Voorst Vader, F.; Erkens, Th. F.; van den Tempel, M. *Trans. Faraday Soc.* **1964**, *60*, 1170−1177.
(53) Danov, K. D.; Kralchevsky, P. A.; Ananthapadmanabhan, K. P.; Lips, A. *J. Colloid Interface Sci.* **2006**, in press.

area and time

$$\tilde{A}(t_d) \equiv A(t_d)/A_0, \quad t_d \equiv t/t_{age} \tag{5.7}$$

see eq 3.1 and Figure 1. In terms of the variables (y,τ), eqs 5.1 and 5.5 acquire the form

$$\frac{\partial c}{\partial \tau} = Dt_{age}\frac{\partial^2 c}{\partial y^2} \quad (\tau > 0, y > 0) \tag{5.8}$$

$$\frac{d}{d\tau}(\Gamma\tilde{A}) = Dt_{age}\frac{\partial c}{\partial y} \quad (\tau > 0, y = 0) \tag{5.9}$$

When solving the diffusion boundary problem, eqs 5.8−5.9, we consider $\tilde{A}$ as a function of τ. Next, we apply Laplace transformation to eq 5.8, and use eqs 5.3 and 5.4; thus, we derive

$$L[c] = \frac{c_\infty}{s} + L[c_s - c_\infty]\exp\left(-y\frac{s^{1/2}}{D^{1/2}t_{age}^{1/2}}\right) \tag{5.10}$$

where L denotes Laplace transformation, s is the Laplace parameter, and $c_s(\tau) \equiv c(y=0,\tau)$ is the subsurface concentration of surfactant. Further, we apply Laplace transformation also to eq 5.9 and use eq 5.10

$$L[\Gamma\tilde{A}] = \frac{\Gamma_0}{s} - (Dt_{age}/s)^{1/2}L[c_s - c_\infty] \tag{5.11}$$

where $\Gamma_0 = \Gamma(\tau = 0)$ is the initial adsorption. The inverse Laplace transformation of eq 5.11, along with the convolution theorem, leads to a version of the Ward-Tordai integral equation[54] for the case of convective diffusion[27]

$$\Gamma\tilde{A} = \Gamma_0 - (Dt_{age}/\pi)^{1/2}\int_0^\tau \frac{c_s(\hat{\tau}) - c_\infty}{(\tau - \hat{\tau})^{1/2}}\,d\hat{\tau} \tag{5.12}$$

Equation 5.12 can be solved if one knows the surfactant adsorption isotherm, $\Gamma(c_s)$, and the area function, $\tilde{A}(t_d)$; see eq 5.6. Thus, one could in principle determine $c_s(\tau)$, as well as $\Gamma(t)$ and $\gamma(t)$. However, this approach is inconvenient for the following reasons. Firstly, the mathematical and computational problem is complicated. Secondly, the experimental determination of the area function $\tilde{A}(t_d)$ from video records of the bubbling process for each separate capillary is labor consuming. Thirdly, the initial adsorption Γ_0 is not well defined and practically unknown. Here, we propose an alternative approach that allows one to avoid all these difficulties when the surfactant concentration is not too low. For this goal, let us represent eq 5.11 in the following equivalent form:

$$\Gamma_{eq}L[\tilde{A}] + L[(\Gamma - \Gamma_{eq})\tilde{A}] = \frac{\Gamma_0}{s} - (Dt_{age}/s)^{1/2}L[c_s - c_\infty] \tag{5.13}$$

The relationship

$$|\Gamma_{eq} - \Gamma| \ll \Gamma_{eq} \tag{5.14}$$

is satisfied in many cases. First of all, eq 5.14 can be applied in the broad concentration domain below the CMC, where the plot of γ_{eq} vs $\log(c)$ is (approximately) linear; see e.g. Figure 11. In this domain, the adsorption is almost saturated, and large variations in c result in very small variations in Γ but in considerable variations in γ (Figure 11). Second, eq 5.14 can be applied to concentrations above the CMC, where adsorption saturation is also present, and the micelles tend to suppress the variations in the monomeric concentration. Third, eq 5.14 is satisfied in the long-time asymptotic region where the adsorption relaxes. Here and hereafter we assume that the surface age is not too low, so that eq 5.14 is satisfied.

When eq 5.14 holds, the second term in the left-hand side of eq 5.13 can be neglected

$$\Gamma_{eq}L[\tilde{A}] \approx \frac{\Gamma_0}{s} - (Dt_{age}/s)^{1/2}L[c_s - c_\infty] \tag{5.15}$$

Further, we transform the left-hand side of eq 5.15 as follows:

$$\Gamma_{eq}L[\tilde{A}] = \frac{\Gamma_{eq}}{s}sL[\tilde{A}] = \frac{\Gamma_{eq}}{s}\left\{1 + L\left[\frac{d\tilde{A}}{d\tau}\right]\right\} \tag{5.16}$$

where the initial condition $\tilde{A}(0) = 1$ has been used. Combining eqs 5.15 and 5.16, we derive

$$L[c_s - c_\infty] = -\frac{\Gamma_{eq} - \Gamma_0}{(Dt_{age}s)^{1/2}} - \frac{\Gamma_{eq}}{(Dt_{age}s)^{1/2}}L\left[\frac{d\tilde{A}}{d\tau}\right] \tag{5.17}$$

Next, we apply inverse Laplace transform to eq 5.17 and use the convolution theorem

$$c_s(\tau) = c_\infty - \frac{\Gamma_{eq} - \Gamma_0}{(\pi Dt_{age}\tau)^{1/2}} - \frac{\Gamma_{eq}}{(\pi Dt_{age})^{1/2}}\int_0^\tau \frac{1}{(\tau - \hat{\tau})^{1/2}}\frac{d}{d\hat{\tau}}[\tilde{A}(\hat{\tau})]\,d\hat{\tau} \tag{5.18}$$

Equation 5.18 will serve as a basis for our further analysis.

5.2. Adsorption at Immobile Interfaces. First, we consider the special case when the fluid interface is immobile. Then, $\tilde{A} \equiv 1$ and $t_{age}\tau = t$, see eqs 5.6 and 5.7. In this special case, eq 5.18 reduces to

$$c_s(t) = c_\infty - \frac{\Gamma_{eq} - \Gamma_0}{(\pi Dt)^{1/2}} \tag{5.19}$$

For small deviations from equilibrium, one could make the following approximations in the Gibbs adsorption equation: $d\gamma \approx \gamma - \gamma_{eq}$ and $(dc_s)/c_s \approx (c_s - c_\infty)/c_\infty$; thus, we obtain

$$\gamma - \gamma_{eq} = -\Gamma_{eq}kT\frac{c_s - c_\infty}{c_\infty} \tag{5.20}$$

Combining eqs 5.19 and 5.20, we obtain

$$\gamma = \gamma_{eq} + \frac{s_{\gamma,0}}{t^{1/2}} \tag{5.21}$$

where

$$s_\gamma,0 \equiv \frac{kT\Gamma_{eq}^{\ 2}}{(\pi D)^{1/2}c_\infty} \tag{5.22}$$

At the last step, we have used the assumption $\Gamma_0 \ll \Gamma_{eq}$, and Γ_0 is neglected.

As an illustration of the applicability of eq 5.21, in Figure A.4 in Appendix A, we have plotted the data from the immobile bubble (IB) method in Figure 2 as γ vs $t^{-1/2}$. It turns out that the data comply very well with straight lines, whose slopes and intercepts are in agreement with the MBPM results in Table 1 (see Appendix A for details).

5.3. Apparatus Constant of the Bubble−Pressure Tensiometer. Let us substitute $t = t_{age}$ in eq 5.18, which is equivalent to setting $t_d = 1$. The result reads

$$c_s(t_{age}) = c_\infty - \frac{(\Gamma_{eq} - \Gamma_0)\lambda_1}{(\pi D t_{age})^{1/2}} - \frac{\Gamma_{eq}\lambda}{(\pi D t_{age})^{1/2}} \qquad (5.23)$$

where, in view of eq 5.6, we have introduced the notations

$$\lambda_1 \equiv \tau_1^{-1/2};\ \tau_1 \equiv \int_0^1 [\tilde{A}(\hat{t}_d)]^2\, d\hat{t}_d \qquad (5.24)$$

$$\lambda \equiv \int_0^{\tau_1} \frac{1}{(\tau_1 - \hat{\tau})^{1/2}} \frac{d}{d\hat{\tau}} [\tilde{A}(\hat{\tau})]\, d\hat{\tau} \qquad (5.25)$$

Usually, $\tilde{A}$ is known as a function of the dimensionless time $t_d = t/t_{age}$, see eq 3.1. For this reason, in eq 5.25, we change the integration variable from $\hat{\tau}$ to t_d

$$\lambda \equiv \int_0^1 \frac{1}{(\tau_1 - \tau)^{1/2}} \frac{d}{dt_d} [\tilde{A}(t_d)]\, dt_d \qquad (5.26)$$

where the dependence $\tau(t_d)$ is given by eq 5.6. Expanding in series the adsorption isotherm, $\Gamma(c_s)$, we obtain

$$\Gamma - \Gamma_{eq} = h_a(c_s - c_\infty), \quad h_a \equiv \left(\frac{\partial \Gamma}{\partial c}\right)_{eq} \qquad (5.27)$$

The substitution of eq 5.23 into eq 5.27 leads to eq 4.1 (with $t = t_{age}$), where

$$s_\Gamma = h_a \frac{(\Gamma_{eq} - \Gamma_0)\lambda_1 + \Gamma_{eq}\lambda}{(\pi D)^{1/2}} \qquad (5.28)$$

The problem considerably simplifies when

$$\frac{\Gamma_{eq} - \Gamma_0}{\Gamma_{eq}} \frac{\lambda_1}{\lambda} \ll 1 \qquad (5.29)$$

As demonstrated below, the latter relation is satisfied for all experimental curves obtained in the present study (Figures 5−8). If eq 5.29 is satisfied, eq 5.23 reduces to

$$c_s(t_{age}) = c_\infty - \frac{\Gamma_{eq}\lambda}{(\pi D t_{age})^{1/2}} \qquad (5.30)$$

Substituting eq 5.30 into eq 5.20, we derive counterparts of eqs 5.21 and 5.22 for the case of expanding interface

$$\gamma = \gamma_{eq} + \frac{s_\gamma}{t_{age}^{1/2}} \qquad (5.31)$$

where

$$s_\gamma \equiv \frac{kT\Gamma_{eq}^2\lambda}{(\pi D)^{1/2} c_\infty} \qquad (5.32)$$

see also eq 5.38. The comparison of eqs 5.22 and 5.32 shows that

$$\lambda = s_\gamma / s_{\gamma,0} \qquad (5.33)$$

The above equation indicates that the dimensionless parameter λ accounts for the effect of the interfacial expansion on the dynamic surface tension. Indeed, eq 5.26, along with eqs 5.6 and 5.24, expresses λ in terms of integrals over the apparatus function $\tilde{A}(t_d)$, which represents the dimensionless time dependence of the bubble interfacial area. As discussed in Section 2.1, $\tilde{A}(t_d)$ is determined by the construction of the given MBPM apparatus, and $\tilde{A}(t_d)$ is independent of the bubbling period, t_{age}, and of the surfactant type and concentration. Hence, the same is true also for λ; that is, λ is determined by the specific apparatus construction. For this reason, λ was termed the apparatus constant.

For a given apparatus, λ could be determined in two different and independent ways. The first way is to use eq 5.26, which requires an empirical equation, like eq 3.1, for the time-dependence of bubble area growth. The second way is to apply eq 5.33, which makes use of the best-fit determination of the parameter s_γ (see eq 4.5 and Tables 1 and 2), whereas $s_{\gamma,0}$ can be determined by either fit of dynamic-surface-tension data for an immobile interface, eq 5.21, or from the values of Γ_{eq}, c_∞, and D, using eq 5.22. Below, we follow the latter approach, i.e., $s_{\gamma,0}$ is calculated from eq 5.22. In other words, we determine $s_{\gamma,0}$ theoretically for an abstract ideal adsorption-relaxation process at an immobile interface, beginning with $\Gamma_0 = 0$. On the other hand, s_γ is determined from the MBPM data for expanding bubbles, without making any assumptions about the value of Γ_0. Consequently, in eq 5.33, we compare the slope parameters, s_γ and $s_{\gamma,0}$, for two different processes, which, in general, begin with different values of Γ_0.

(1) Determination of λ from eq 5.26 using the Experimental Dependence $A(t_d)$. Because the bubble area, $A(t_d)$, strongly increases for $t_d = t/t_{age} \to 1$, we fitted the data in Figure 1b by an empirical expression, eq 3.1, which contains $\ln(1 - t_d)$ and its powers. The latter function has an integrable singularity at $t_d = 1$. To avoid computational problems, without any perceptible loss of accuracy, one could stop the integration in eq 5.26 at the point of hemispherical bubble, where $A/A_0 = \tilde{A} = 2$ (see Figure 1b), thus avoiding the singularity at $t_d = 1$. Correspondingly, eq 5.26 acquires the form

$$\lambda \approx \int_1^2 \frac{1}{(\tau_1 - \tau)^{1/2}} d\tilde{A} \qquad (5.34)$$

Equation 3.1 gives $\tilde{A}(t_d)$, and eq 5.6 gives $\tau(t_d)$. The latter two dependencies determine the function $\tau(\tilde{A})$ in parametric form. The latter dependence was used to solve numerically the integral in eq 5.34. Thus, for $\tilde{A}(t_d)$ given by eq 3.1 (and Figure 1b), we calculate

$$\lambda = 6.074, \quad \lambda_1 = 0.8269 \qquad (5.35)$$

The ratio $(\Gamma_{eq} - \Gamma_0)/\Gamma_{eq}$ is smaller than 1, and it becomes even smaller with the rise of surfactant concentration, which leads to a greater Γ_0. (Here, Γ_0 refers to the initial adsorption in the MBPM experiment.) Thus, we have $\lambda_1/\lambda < 0.8269/6.074 = 0.136$; the ratio in eq 5.29 is even smaller because of the factor $(\Gamma_{eq} - \Gamma_0)/\Gamma_{eq} < 1$. This is confirmed by the average experimental value, $\lambda = 6.07 \pm 0.01$ (Table 5), which is very close to the theoretical value, $\lambda = 6.074$ (from eq 5.34). The latter coincidence indicates that the relation 5.29 is really satisfied and that the term with λ_1 in eq 5.23 is negligible.

(2) Determination of λ from eq 5.33 using s_γ from the MBPM Data Fits. Table 5 contains data from our MBPM experiments (Figures 5−8) for the concentrations ≤CMC. (For concentrations >CMC, the interpretation of the data is given in Section 6.) The equilibrium surfactant adsorption, $\Gamma_{eq} = \Gamma_1$, is calculated with the help of eqs 4.9−4.11 using the parameter values in Table 3. Next, $s_{\gamma,0}$ is calculated from a generalized form of eq 5.22, which is applicable to both nonionic and ionic surfactants[53]

$$s_{\gamma,0} \equiv \frac{kT\Gamma_{eq}^{\ 2}}{(\pi D)^{1/2}\gamma_{\pm}\hat{c}_{\infty}} \tag{5.36}$$

For nonionic surfactants, the activity coefficient is $\gamma_{\pm} \approx 1$ and $\hat{c}_{\infty} = c_{\infty}$ is the bulk surfactant concentration. For ionic surfactants, $\gamma_{\pm}$ can be estimated by means of eq 4.12, whereas

$$\frac{1}{\hat{c}_{\infty}} = \frac{1}{c_{1\infty}} + \frac{1}{c_{2\infty}} \quad \text{(ionic surfactant)} \tag{5.37}$$

where $c_{1\infty}$ and $c_{2\infty}$ are the bulk concentrations of surfactant ions and counterions. In addition, for ionic surfactants D is an effective diffusion coefficient, which has to be calculated from eqs B.1−B.7 in Appendix B. D is related to the diffusivities of the surfactant ions, counterions, and coions, D_1, D_2, and D_3, and depends on the concentrations $c_{1\infty}$ and $c_{2\infty}$. The used values of D_1, D_2, and D_3 are given in Appendix B; see also refs 60−62.

At high salt concentrations ($c_{2\infty} \gg c_{1\infty}$), eq 5.37 yields $\hat{c}_{\infty} \approx c_{1\infty}$ and eq B.1 yields $D = D_1$. This is the case of SDS and DTAB + 100 mM added electrolyte (Figures 6 and 8). However, in the case of 5 and 10 mM added electrolyte (Figures 5 and 7), we used the full set of eqs B.1−B.7 in Appendix B to calculate D.

It can be proven that the generalization of eq 5.32 to the case of arbitrary ionic surfactant solutions is[53]

$$s_{\gamma} \equiv \frac{kT\Gamma_{eq}^{\ 2}\lambda}{(\pi D)^{1/2}\gamma_{\pm}\hat{c}_{\infty}} \tag{5.38}$$

where $\hat{c}_{\infty}$ and D are defined by eqs 5.37 and B.1, respectively. To obtain eq 5.38, one could formally multiply eq 5.36 by λ and use the relation $s_{\gamma} = \lambda s_{\gamma,0}$.

In Table 5, the values of Γ_{eq} and $s_{\gamma,0}$ are calculated from eqs 4.9−4.11 and 5.36 as explained above. The values of s_{γ} are taken from Tables 1 and 2. The apparatus constant is calculated in accordance with eq 5.33: $\lambda = s_{\gamma}/s_{\gamma,0}$. The last column shows the relative deviation of the experimental value from the theoretical one: $r_{\lambda} = |\lambda - 6.074|/6.074$, see eq 5.35. As already mentioned, the mean value for all runs in Table 5, $\lambda = 6.07 \pm 0.01$, is very close to the theoretical value $\lambda = 6.074$ (eq 5.35). The implications of these results are discussed below.

5.4. Discussion. As mentioned above, the apparatus constant, λ, characterizes a given MBPM tensiometer and could depend on the used capillary (hydrophilic or hydrophobic). On the other hand, λ is independent of the surfactant type and concentration, and on the bubbling period.

Because $\lambda = s_{\gamma}/s_{\gamma,0}$, one can represent eq 5.31 in the form

$$\gamma = \gamma_{eq} + \frac{s_{\gamma,0}}{t_u^{1/2}} \tag{5.39}$$

where $t_u = t_{age}/\lambda^2$. In view of eq 5.21, eq 5.39 describes the dynamic surface tension of an (initially perturbed) immobile bubble of age $t = t_u$. In terms of t_u, a dynamic surface tension curve obtained by MBPM becomes identical to the relaxation curve of γ for an immobile interface. In other words, t_u is the age of an immobile, initially clean fluid interface with the same instantaneous surface tension as that determined by the MBPM. This fact is illustrated in Figure 2 and its importance is discussed in Section 2.2. In particular, the knowledge of λ makes the results obtained by a given MBPM setup comparable with that obtained by other MBPM tensiometers or by other methods for measurement of dynamic surface tension.

Table 5. Apparatus Constant, λ, Determined for Concentrations ≤ CMC (Figures 5−8)

$C_{surfactant}$ (mM)	$\tilde{\Gamma}_{eq}$ (μmol/m^2)	$s_{\gamma,0}$ (mN·m^{-1}·s$^{1/2}$)	s_{γ} (mN·m^{-1}·s$^{1/2}$)	$\lambda = s_{\gamma}/s_{\gamma,0}$	$1000\times r_{\lambda}$
		SDS + 10 mM NaCl			
0.1	0.907	0.5529	3.36	6.077	0.5
0.5	2.653	0.9789	5.95	6.078	0.7
1	3.320	0.7962	4.83	6.066	1.3
2	3.762	0.5451	3.31	6.073	0.2
3	3.955	0.4231	2.57	6.075	0.1
		SDS + 100 mM NaCl			
0.2	3.434	4.5602	27.7	6.074	0.0
0.5	3.863	2.3155	14.0	6.046	4.6
0.75	3.999	1.6583	10.1	6.091	2.7
1	4.082	1.2989	7.89	6.075	0.1
		DTAB + 5 mM NaBr			
1	1.690	0.2219	1.35	6.083	1.5
2	2.360	0.2361	1.43	6.057	2.9
3	2.687	0.2172	1.32	6.079	0.8
5	3.013	0.1782	1.08	6.060	2.3
7	3.182	0.1501	0.912	6.075	0.2
10	3.330	0.1217	0.738	6.066	1.4
12	3.395	0.1082	0.657	6.069	0.8
		DTAB + 100 mM NaBr			
2	3.262	0.4383	2.66	6.068	1.0
3	3.354	0.3115	1.89	6.068	1.0
4	3.411	0.2436	1.48	6.075	0.2
avg.				$\lambda = 6.07 \pm 0.01$	

In Figures 5b, 6b, 7b, and 8b, we have shown the universal surface age t_u (the upper horizontal axis). The relationship $t_u = t_{age}/\lambda^2$ (eq 2.1) is valid in the whole region, in which the experimental data can be fitted by means of eq 4.5 (see the solid lines in Figures 5−8). In our case (Table 5), $\lambda = 6.07$, and correspondingly, in Figures 5b−8b, we have $t_u \approx t_{age}/37$. As seen in these figures, the earliest universal ages are $t_u \approx 0.3$ ms. The latter result confirms that MBPM is one of the fast methods for dynamic surface tension measurements. A comparison of different dynamic methods could be found elsewhere.[23,29]

To determine λ for a given MBPM setup, one could use the following procedure.

(1) One has to choose several reference surfactant solutions. For example, one could choose any of the systems in Table 5; for all of them, the values of $s_{\gamma,0}$ are available in this table. For other systems, the value of $s_{\gamma,0}$ could be determined as explained above.

(2) For the selected reference solutions (of concentrations ≤CMC), dynamic surface tension curves, $\gamma(t_{age})$, like those in Figures 5−8, are obtained. The data are fitted by means of eq 4.5, and s_{γ} is determined for each experimental curve. (One could also fit the data by eq 4.8 and then calculate $s_{\gamma} = b_{\gamma} - a_{\gamma}\gamma_{eq}$.)

(3) Finally, the apparatus constant is obtained by means of eq 5.33: $\lambda = s_{\gamma}/s_{\gamma,0}$. For a better statistics, it is preferable to determine λ for several different surfactant concentrations, as in Table 5, and then to take the mean arithmetic λ.

The above procedure is much simpler and less time-consuming than the alternative procedure based on taking photographs of the bubble expansion process (Figure 3), determining the bubble area as a function of time, $A(t_d)$, and finally, calculating λ by integration in eq 5.26 or 5.34; see also Figure 1.

Note that a given MBPM setup can be characterized with a single apparatus constant, λ, only when the relation 5.29 is satisfied. Otherwise, s_{γ} depends on two additional parameters, λ_1 and Γ_0, which are not easy to be determined; compare eqs 5.23 and 5.30. In order for eq 5.29 to be satisfied, λ should be sufficiently large. Equation 5.26 implies that large λ values are

obtained when the function $\tilde{A}(t_d)$ steeply increases for $t \to t_d$, as it is in Figure 1b. In such a case, the derivative in eq 5.26 is large in the region where the denominator $(\tau_1 - \tau)^{1/2} \to 0$, which leads to a greater value of the integral, which expresses λ.

Finally, we should note that if one knows λ for a given MBPM setup, from the experimental value of s_γ and eq 5.38, one could determine either Γ_{eq} or D, if one of the latter two parameters is known. Of course, both Γ_{eq} and D could be determined by other methods, different from the MBPM. In this respect, the MBPM results could be more informative in the case of concentrations above the CMC, which is considered in the next section.

6. Interpretation of the Dynamic Surface Tension above the CMC

Four distinct kinetic regimes of adsorption from micellar solutions, called AB, BC, CD, and DE, have been established.[34,35] In regime AB, the fast micellar process governs the adsorption kinetics. In regime BC, the adsorption occurs under diffusion control, because the fast micellar process is equilibrated, while the effect of the slow process is negligible. In regime CD, the slow micellar process governs the adsorption kinetics. In regime DE, the adsorption occurs under diffusion control, because both the fast and slow micellar processes are equilibrated. Note that only the regimes BC and DE correspond to purely diffusion processes. For the regimes AB and CD, an additional source term related to the micellar kinetics should be included in eq 5.1. (The latter case is out of the scope of the present study.)

For the diffusion regimes BC and DE, following ref 34, one can prove (Appendix C) that eq 5.31 is applicable also for concentrations above the CMC, with s_γ defined as follows:

$$s_\gamma \equiv \frac{kT\Gamma_{eq}^{\ 2}\lambda}{(\pi D_{eff})^{1/2}\mathrm{CMC}} \tag{6.1}$$

Here D_{eff} is an effective diffusion coefficient for micellar solutions. D_{eff}, which accounts for the contribution of the micelles in the surfactant transport, has been introduced by Joos et al.[55,56] The division of eq 6.1 by eq 5.32 at $c_\infty = \mathrm{CMC}$, yields

$$\frac{D_{eff}}{D} = \frac{s_{\gamma,\mathrm{CMC}}^{\ 2}}{s_\gamma^{\ 2}} \tag{6.2}$$

where $s_{\gamma,\mathrm{CMC}}$ is the value of s_γ measured at the CMC and D is the diffusivity of the surfactant monomers calculated from eqs B.1−B.7. (As mentioned above, for nonionic surfactants and for ionic surfactants at high concentration of added electrolyte, we have $D \approx D_1$.) Taking $s_{\gamma,\mathrm{CMC}}$ and s_γ from Tables 1 and 2 for concentrations ≥CMC, from eq 6.2, we calculate D_{eff}/D. The results are plotted in Figure 13 versus the quantity

$$\beta \equiv \frac{C_{tot} - \mathrm{CMC}}{\mathrm{CMC}} \tag{6.3}$$

where C_{tot} is the total surfactant concentration. To obtain D_{eff}/D, we do not need the value of the apparatus constant, λ: the latter cancels when taking the ratio of eqs 6.1 and 5.32, supposedly λ is independent of the surfactant concentration.

The data in Figure 13 indicate that the experimental D_{eff}/D considerably increases with the rise of surfactant concentration, starting from 1 at the CMC, up to ≈ 95 at 100 mM DTAB + 100 mM NaBr ($\beta \approx 22.5$). The errors of the determined D_{eff}/D are relatively small because of the small errors in s_γ; see Tables 1 and 2.

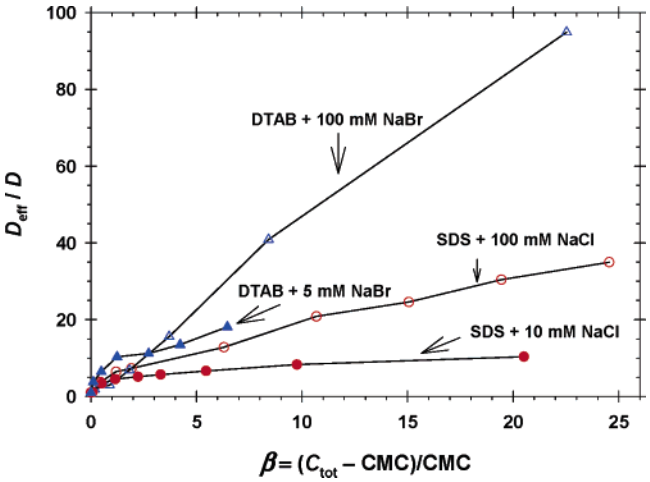

Figure 13. Plot of the dimensionless effective diffusivity of the micellar solution, D_{eff}/D, vs β, calculated my means of eq 6.2 from the data for s_γ in Tables 1 and 2 for $C_{tot} \geq$ CMC. The lines are guides to the eye.

In general, we do not know which of the four possible kinetic regimes of adsorption above the CMC is observed in a given experiment. Here, we will check whether the data in Figure 13 could be interpreted in terms of the diffusional regime BC or DE, for which we have[34,35]

$$\frac{D_{eff}}{D} = \frac{D_{BC}}{D} = \left(1 + \frac{\sigma_{eq}^{\ 2}}{m_{eq}}\beta\right)\left(1 + \frac{\sigma_{eq}^{\ 2}}{m_{eq}}\frac{D_m}{D}\beta\right) \tag{6.4}$$

$$\frac{D_{eff}}{D} = \frac{D_{DE}}{D} = \left(1 + \frac{m_{eq}^{\ 2} + \sigma_{eq}^{\ 2}}{m_{eq}}\beta\right)\left(1 + \frac{m_{eq}^{\ 2} + \sigma_{eq}^{\ 2}}{m_{eq}}\frac{D_m}{D}\beta\right) \tag{6.5}$$

Here D_{BC} and D_{DE} are the values of D_{eff} for the respective regime; D_m is the average diffusion coefficient of the micelles; m_{eq} and σ_{eq} are parameters of the equilibrium micelle size distribution, which has been assumed to have Gaussian shape,[33−35] after Aniansson and Wall[57]

$$c_n = \frac{C_m}{\sqrt{2\pi}\sigma_{eq}}\exp\left[-\frac{(n - m_{eq})^2}{2\sigma_{eq}^{\ 2}}\right] \tag{6.6}$$

Here, c_n is the concentration of micelles of aggregation number n; C_m is the total concentration of the abundant micelles; m_{eq} is their equilibrium mean aggregation number; σ_{eq} is the standard deviation of the Gaussian distribution, which characterizes the polydispersity of the abundant micelles at equilibrium. (If we formally set $\sigma_{eq}^{\ 2}/m_{eq} = 1$, eqs 6.4 and 6.5 reduce to the expressions for D_{BC} and D_{DE} in the works by Joos[55,56] and Lucassen.[58])

To check whether the kinetic regime is DE, we substitute typical parameter values in eq 6.5

$$\frac{D_{DE}}{D} = (1 + 70 \times 20)(1 + 70 \times 0.2 \times 20) = 393681 \tag{6.7}$$

In the above estimate, we have neglected $(\sigma_{eq}/m_{eq})^2 \ll 1$, and we have substituted $m_{eq} = 70$, $\beta = 20$, and $D_m/D = 0.2$. The value

(54) Ward, A. F. H.; Tordai, L. *J. Chem. Phys.* **1946**, *14*, 453−461.
(55) Joos P.; Van Hunsel J. *Colloids Surf.* **1988**, *33*, 99−108.
(56) Li, B.; Joos, P.; van Uffelen, M. *J. Colloid Interface Sci.* **1995**, *171*, 270−275.
(57) Aniansson, E. A. G.; Wall, S. N. *J. Phys. Chem.* **1974**, *78*, 1024−1030.
(58) Lucassen, J. *Faraday Discuss. Chem. Soc.* **1975**, *59*, 76−87.

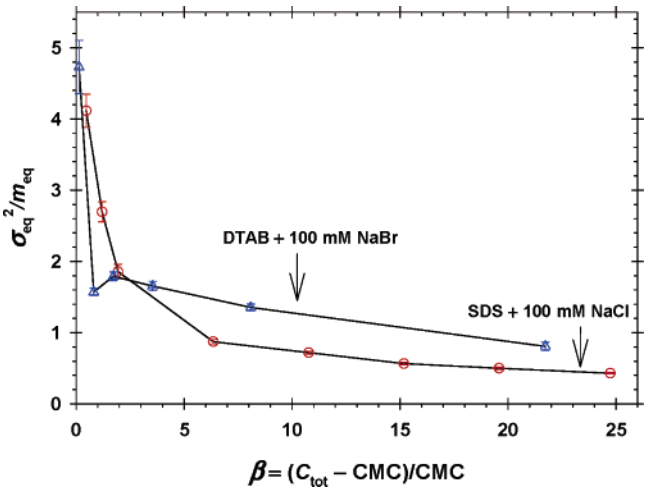

Figure 14. Plot of σ_{eq}^2 vs β calculated from the data for D_{eff}/D in Figure 13 with the help of eq 6.4 for $D_m/D = 0.2$. The lines are guides to the eye.

of D_{DE}/D in eq 6.7 is much greater than the experimental values of D_{eff}/D in Figure 13; consequently, the kinetic regime cannot be DE.

On the other hand, a similar estimate of D_{BC}/D from eq 6.4 gives reasonable values. To demonstrate that, from the experimental values of D_{eff}/D in Figure 13, we calculated σ_{eq}^2/m_{eq} by means of eq 6.4. $D_m/D = 0.2$ is used again.[35,56,58] The results for σ_{eq}^2/m_{eq} are shown in Figure 14. Data for the solutions containing 100 mM added electrolyte are only presented because eqs 6.4 and 6.5 are originally derived[34,35] for nonionic surfactants and are expected to be valid for ionic surfactants only at high salt concentrations. Values $0.4 < \sigma_{eq}^2/m_{eq} < 2$ seem reasonable. The values $\sigma_{eq}^2/m_{eq} > 2$ at the smallest β indicate that at the lowest micellar concentrations we are dealing with a rudimentary kinetic regime,[34,35] rather than with the diffusional regime BC. In other words, for the smallest β, eq 6.4 is inapplicable.

In Figure 14, the values of σ_{eq}^2/m_{eq} for $\beta \geq 2$ seem reasonable. For example, at $\beta = 10$, we have $\sigma_{eq}^2/m_{eq} \approx 0.75$ and 1.3 for SDS and DTAB, respectively, which gives micellar polydispersity $\sigma_{eq} = 7.2$ and 9.5 monomers per micelle, if we assume $m_{eq} \approx 70$ for both surfactants. This result indicates that for $\beta \geq 2$ we are dealing with the diffusional kinetic regime BC. The trend of σ_{eq}^2/m_{eq} to slightly decrease with the rise of the surfactant concentration, characterized by β, could be attributed to the tendency of the mean micellar aggregation number, m_{eq}, to increase with β.[59]

7. Summary and Concluding Remarks

Here, based on the theoretical analysis of data for two ionic surfactants (SDS and DTAB, Figures 5−8), we developed a new approach for quantitative interpretation of the results of the maximum bubble pressure method (MBPM). A given MBPM tensiometer is characterized by an apparatus function, $A(t_d)$, and by an apparatus constant, λ. The former represents the time dependence of the bubble surface area. It was measured by video microscopy (Figures 1 and 3), and it was found to be independent of the surfactant type and concentration but dependent on the specific MBPM setup. The same is true for the apparatus constant, λ, which is expressed as an integral over $A(t_d)$, eq 5.26. If the construction of the MBPM tensiometer is appropriate to ensure fast bubble expansion at the moment of the maximum pressure (Figure 1b), the criterion 5.29 is satisfied, and the experimental results depend on $A(t_d)$ only through λ. This finding makes the interpretation of the MBPM data much easier insofar as for a given setup, λ can be measured by calibration with reference solutions (see Table 5 and Section 5.4), whereas the determination of $A(t_d)$ demands use of video microscopy and image analysis and represents a difficult task, especially at the high bubbling frequencies. Having determined λ, one could plot the experimental dynamic surface tension vs the universal surface age, $t_u = t_{age}/\lambda$ (Figures 5b−8b). Such a plot is independent of the specific MBPM setup and produces dynamic surface tension curves that are universal characteristics of the investigated solutions (Figure 2).

A new equation for processing the dynamic surface tension is proposed (see eqs 4.5 and 4.8). Excellent fits of the experimental results are obtained at concentrations below and above the CMC (Tables 1 and 2, and Figures 5−9). The equilibrium surface tension determined from the MBPM data fits agrees very well with results of independent experiments (Figure 11, and Table A.1 in Appendix A). At concentrations below the CMC, the slope coefficient, s_γ, determined from the fits, allows one to determine the apparatus constant, λ, the equilibrium adsorption, Γ_{eq}, or the surfactant diffusivity, D, if two of the latter three parameters are known; see eq 5.32. At concentrations above the CMC, the analysis of the MBPM data enables one to reveal which of the four possible kinetic regimes of adsorption is realized. In particular, the slope coefficient, s_γ, yields the effective diffusivity of the surfactant in the micellar solution, D_{eff}; see eq 6.2. The analysis of the concentration dependence of D_{eff} (Figures 13 and 14) indicates that for the investigated solutions of SDS and DTAB the kinetic regime is BC, i.e., the fast micellar process is equilibrated, while the slow micellar process is negligible. In principle, the maximum-bubble-pressure method could allow one to detect and identify also other kinetic regimes of adsorption from micellar solutions.

Upgraded with the developed approach for quantitative data interpretation, the MBPM becomes a useful tool for investigation of fast adsorption processes at concentrations around and above the CMC, which are accessible to few experimental methods. (The smallest universal surface age achieved in the reported experiments is 0.3 ms.) Some of the parameters, which can be determined by MBPM at concentrations ≤CMC (such as Γ_{eq}, γ_{eq}, and D), could be measured also by other methods. The MBPM could find interesting applications to concentrations above the CMC, where different kinetic regimes of adsorption could take place, as well as to mixed surfactant−surfactant and surfactant−polymer solutions.

Acknowledgment. We gratefully acknowledge the support of Unilever Research & Development, Trumbull, Connecticut, and of the Bulgarian NSF, Program "Development of Scientific Infrastructure".

Supporting Information Available: Experimental Supporting Information (Appendix A); calculation of D in eqs 5.36 and 5.38 for ionic surfactants below the CMC (Appendix B), and dynamic surface tension of micellar solutions: derivation of eq 6.1 (Appendix C). This material is available free of charge via the Internet at http://pubs.acs.org.

LA061239H

(59) Bergström, M.; Pedersen, J. S. *Phys. Chem. Chem. Phys.* **1999**, *1*, 4437−4446.
(60) Kamenka, N.; Lindman, B.; Brun, B. *Colloid Polym. Sci.* **1974**, *252*, 144−152.
(61) Landau, L. D.; Lifshitz, E. M. Fluid Mechanics. In *Course of Theoretical Physics*; Pergamon Press: Oxford, U.K., 1982; Vol. 6.
(62) Israelachvili, J. N. *Intermolecular and Surface Forces*; Academic Press: London, 1992; p 55.

Supporting Information

For the Paper: The Maximum Bubble Pressure Method:
Universal Surface Age and Transport Mechanisms in Surfactant Solutions

Authors: ***Nikolay C. Christov, Krassimir D. Danov, Peter A. Kralchevsky, Kavssery P. Ananthapadmanabhan, and Alex Lips***

(The reference numbers are the same as in the main paper; see the reference list therein)

Appendix A. Experimental Supporting Information

One of the main problems with MBPM is that different experimental setups give different experimental curves $\gamma(t_{age})$.[24] Moreover, the same setup gives different $\gamma(t_{age})$-curves if different (hydrophilic and hydrophobic) capillaries are used.[17] This is illustrated in Figure A.1 with data obtained by means of two experimental setups. The first one is an apparatus constructed and described in ref 17; data obtained by this setup (the square symbols in Figure A.1) are taken from ref 26. The second MBPM apparatus is the commercial tensiometer Krüss BP2. As usual,[28,29] the data are plotted as γ vs. $(t_{age})^{-1/2}$. One sees that the experimental curves obtained at the same surfactant and salt concentrations by two different setups are rather different. The main difference is in the shape of the curves, including their slopes at $(t_{age})^{-1/2}\rightarrow 0$. On the other hand the intercept at $(t_{age})^{-1/2} = 0$, which gives the equilibrium surface tension, is not so different for the two setups.

As mentioned in relation to Figure A.1, the data for the dynamic surface tension produced by the MBPM are usually plotted as γ vs. $t_{age}^{-1/2}$, and the equilibrium surface tension, γ_{eq}, is determined from the intercept, while the asymptotic slope (at $t_{age}^{-1/2}\rightarrow 0$) is subjected to theoretical analysis.[29] However, as illustrated in Figure A.2, this procedure gives uncertain values of the asymptotic slope and intercept. One sees that the data for $t_{age}^{-1/2} > 1$ $s^{-1/2}$ comply well with a straight line. The same is true for the data for $t_{age}^{-1/2} < 1$ $s^{-1/2}$ (the inset in Figure A.2). The slopes of the two lines are markedly different, whereas the difference between the intercepts is of the order of the experimental error of γ_{eq}, which is typically ±0.1 mN/m. The difference is especially pronounced for the slopes. Because the adsorption rate depends on both surfactant type and concentration, one could not know in advance in which range of bubbling periods the experimental dependence γ vs. $t_{age}^{-1/2}$ reduces to a straight-line asymptote. Such uncertainty often appears when a curvilinear experimental dependence has to be asymptotically fitted with a straight line.

(a)

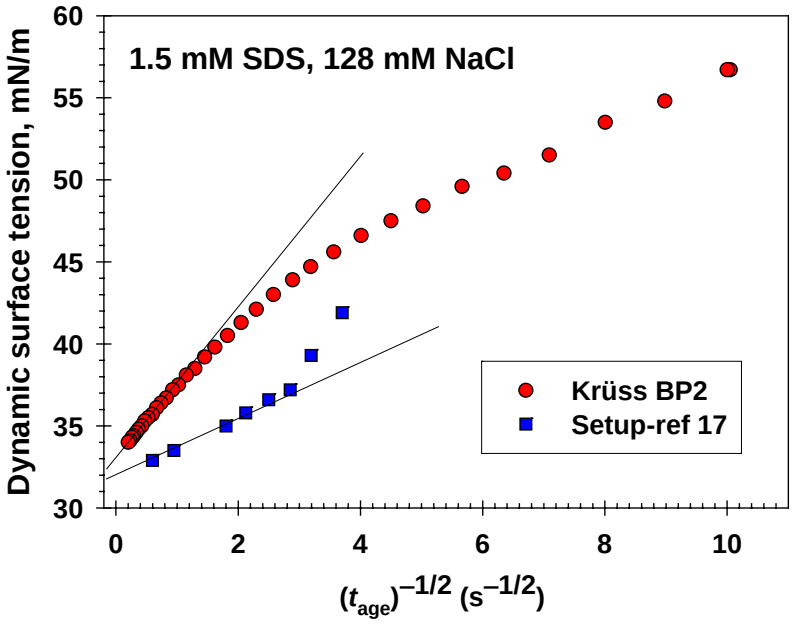

(b)

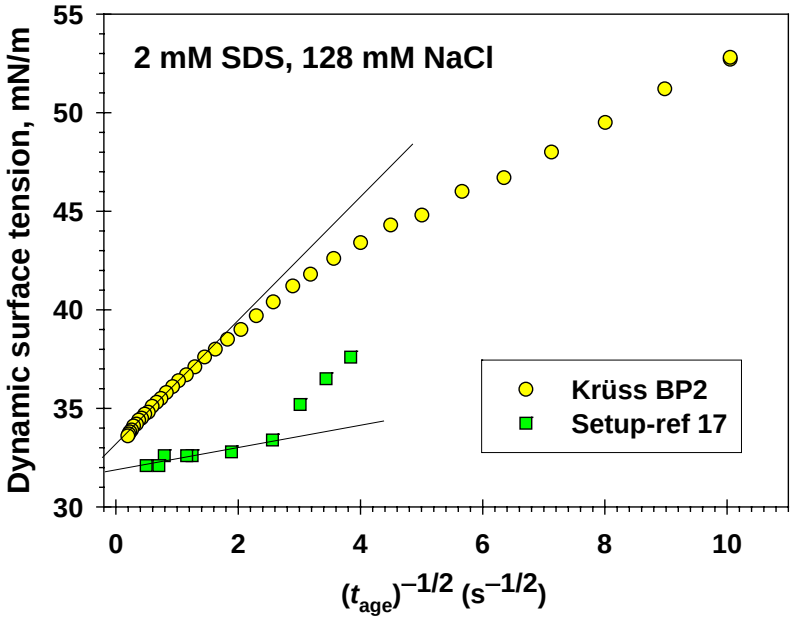

Figure A.1. Plot of the dynamic surface tension, γ, vs. $(t_{age})^{-1/2}$ for data obtained by means of two MBPM setups, denoted in the figure: (a) 1.5 mM SDS + 128 mM NaCl; (b) 2 mM SDS + 128 mM NaCl.

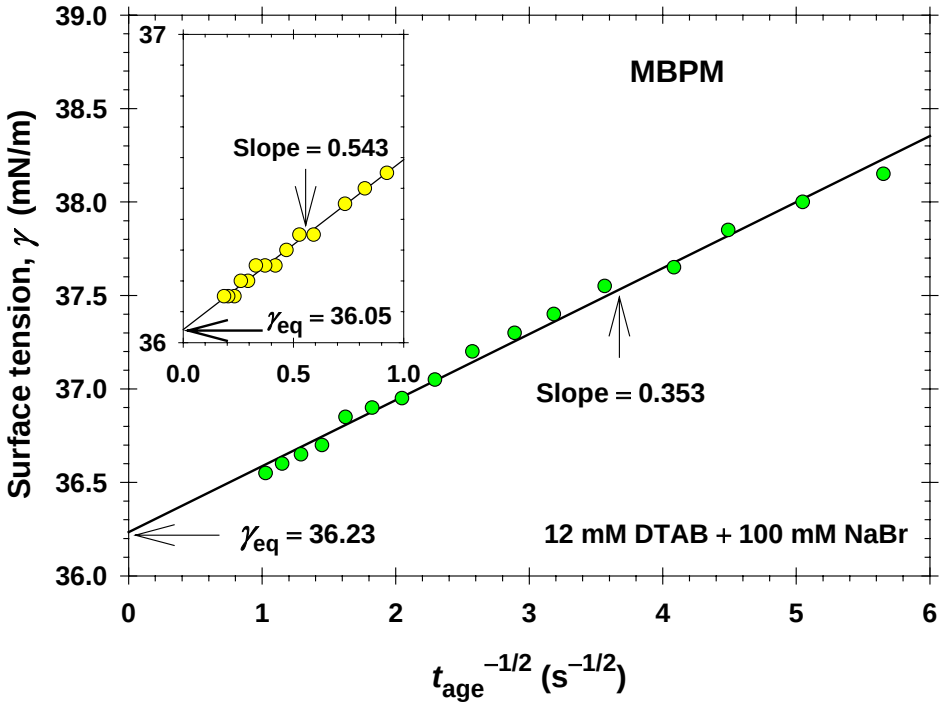

Figure A.2. Plot of data for γ vs. $t_{age}^{-1/2}$ obtained by MBPM for 12 mM DTAB + 100 mM NaBr. For $t_{age}^{-1/2} > 1$ $s^{-1/2}$, the slope of the linear regression is 0.353 $mN.m^{-1}.s^{1/2}$, whereas for $t_{age}^{-1/2} < 1$ $s^{-1/2}$ (the inset), the slope is 0.543 $mN.m^{-1}.s^{1/2}$.

Figure A.3 shows typical dynamic-surface-tension curves, $\gamma(t_{age})$, obtained by means of the two types of capillaries, those hydrophobized by silicone oil and HMDS. We recall that for the Krüss BP2 tensiometer, the surface age, t_{age}, is defined as the time interval between the minimal measured pressure, identified with the bubble formation, and the maximum pressure, which marks the onset of the spontaneous bubble detachment. The registered value of γ corresponds to the latter moment. Each curve $\gamma(t_{age})$ is obtained by variation of the bubbling period. Figure A.3 shows that there is a difference between the experimental $\gamma(t_{age})$-curves obtained by means of the capillaries treated by silicone oil and HMDS. In the former case (Figure 3 in the main paper), the curves are relatively smooth, while in the latter case (Figure 4 in the main paper) the curves exhibit some undulations, which are probably due to the more complicated regime of bubble release. In our basic experiments (Figures 5–8 in the main paper), we used the capillary hydrophobized by silicone oil, which provides a regular regime of bubble formation (Figures 1b and 3 in the main paper), described by the apparatus function, $A(t_d)$, given by eq 3.1 in the main paper.

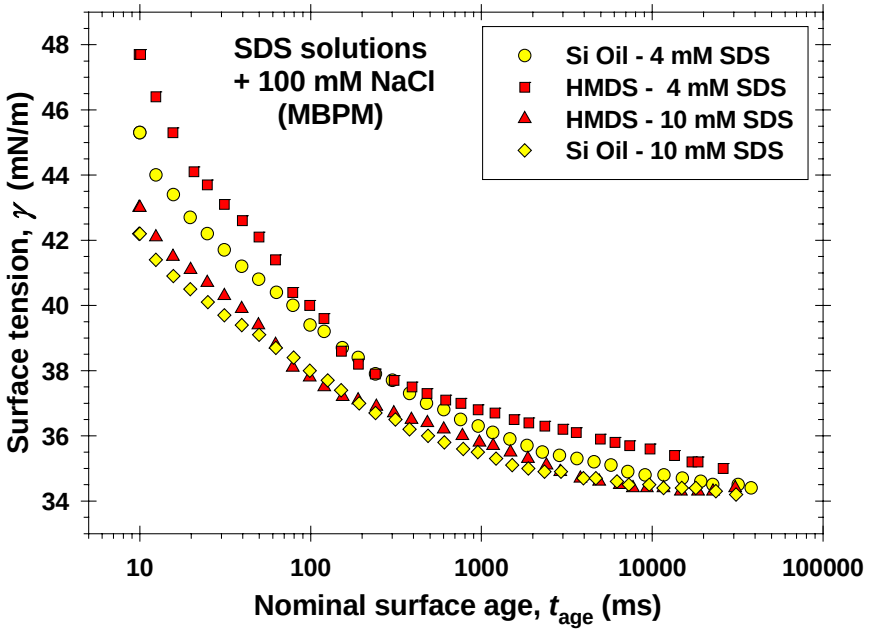

Figure A.3. Comparison of dynamic surface tension curves, $\gamma(t_{age})$, obtained by the two capillaries, one of them hydrophobized by silicone oil (Figure 3 in the main paper), and the other one – by HMDS (Figure 4 in the main paper).

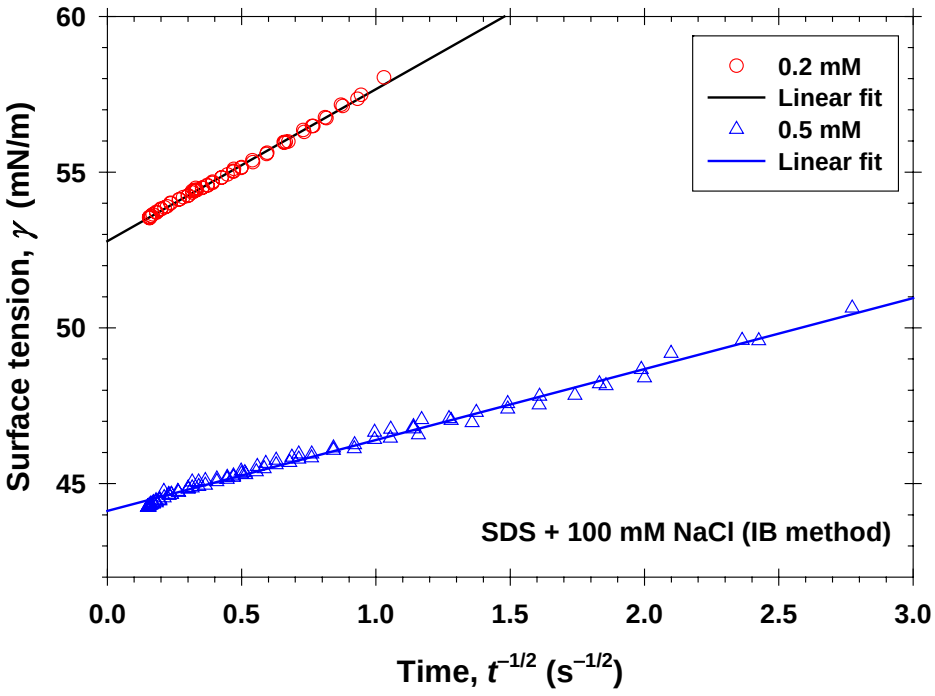

Figure A.4. Plot of the data from the immobile bubble (IB) method in Figure 3 as γ vs. $t^{-1/2}$ in accordance with eq 5.21 ($t = t_{age}$). The SDS concentrations are 0.2 and 0.5 mM, and the NaCl concentration is 100 mM.

As an illustration of the applicability of eq 5.21 in the main paper,

$$\gamma = \gamma_{\rm eq} + \frac{s_{\gamma,0}}{t^{1/2}} \tag{5.21}$$

in Figure A.4 we have plotted the data from the immobile bubble (IB) method in Figure 3 (main paper) as γ vs. $t^{-1/2}$. As seen in Figure A.4, the data comply very well with straight lines. The intercept and the slope of these lines, $\gamma_{\rm eq}$ and $s_{\gamma,0}$, are listed in Table A.1, where they are compared with the values of $\gamma_{\rm eq}$ and s_γ, for the same SDS concentrations in Table 1 of the main paper (MBPM). One sees that the values of $\gamma_{\rm eq}$ determined by the MBPM and IB method practically coincide (Table A.1). On the other hand, s_γ is systematically greater than $s_{\gamma,0}$. The ratio $\lambda \equiv s_\gamma/s_{\gamma,0}$ is about 6. As demonstrated in section 5.3 of the main paper, the quantity λ is, in fact, the apparatus constant of the used MBPM setup.

Table A.1. Comparison of the MBPM and IB Methods for Solutions of SDS + 100 mM NaCl

$C_{\rm SDS}$ (mM)	$\gamma_{\rm eq}$ [IB] (mN/m)	$\gamma_{\rm eq}$ [MBPM] (mN/m)	$s_{\gamma,0}$ [IB] (mN.s$^{1/2}$.m^{-1})	s_γ [MBPM] (mN.s$^{1/2}$.m^{-1})	$\lambda \equiv s_\gamma/s_{\gamma,0}$
0.2	52.78	53.10	4.88	27.7	5.7
0.5	44.13	44.37	2.28	14.0	6.1

Appendix B: Calculation of *D* in Eqs 5.36 and 5.38 for Ionic Surfactants below the CMC

Here, as usual, the components 1, 2 and 3 are, correspondingly, the surfactant ions, counterions and coions. For example, in the case of SDS + NaCl, these are, respectively, DS^-, Na^+, and Cl^-. In the case of DTAB + NaBr, components 1, 2 and 3 are, respectively, DTA^+, Br^-, and Na^+. The corresponding bulk concentrations and diffusivities are denoted by $c_{1\infty}$, $c_{2\infty}$, $c_{3\infty}$, and D_1, D_2, D_3. Note that because of the solution's electroneutrality, we have $c_{2\infty} = c_{1\infty} + c_{3\infty}$.

In ref 53, by analysis of the diffusion of the ionic species across the electric double layer, eqs 5.36 and 5.38 in the present paper were derived. In these equations, D is an effective diffusion coefficient of the ionic surfactant defined as follows:[53]

$$D = (a_{11} + a_{33} + 2a^{1/2})q^2 \tag{B.1}$$

where

$$q = \frac{(c_{1\infty} + c_{2\infty})a^{1/2}}{(a_{33} - a_{31} + a^{1/2})c_{1\infty} + (a_{33} + a^{1/2})c_{2\infty}} \tag{B.2}$$

$$a = \frac{2c_{2\infty}}{B} D_1 D_2 D_3 \tag{B.3}$$

$$B = D_1 c_{1\infty} + D_2 c_{2\infty} + D_3 c_{3\infty} \tag{B.4}$$

$$a_{11} = D_1 + \frac{D_2 - D_1}{B} D_1 c_{1\infty} \tag{B.5}$$

$$a_{31} = \frac{D_2 - D_1}{B} D_3 c_{3\infty} \tag{B.6}$$

$$a_{33} = D_3 + \frac{D_2 - D_3}{B} D_3 c_{3\infty} \tag{B.7}$$

In the special case of *high salt* concentration or *low surfactant* concentration, $c_{1\infty}/c_{3\infty} << 1$, eq B.1 reduces to:[53]

$$D_{\text{eff}} \approx D_1 \qquad (c_{1\infty} / c_{3\infty} << 1) \tag{B.8}$$

In the *absence* of non-amphiphilic electrolyte ($c_{3\infty} = 0$), eq B.1 acquires the form:[53]

$$\frac{1}{D_{\text{eff}}} = \frac{1}{2}\left(\frac{1}{D_1} + \frac{1}{D_2}\right) \qquad (c_{3\infty} = 0) \tag{B.9}$$

In the general case, one has to calculate D_{eff} from eq B.1, along with eqs B.2 – B.7. The latter equations are applicable for concentrations below the CMC.

Here, in our calculations we used the following values of the diffusion coefficients. For SDS, the surfactant diffusivity is $D_1 = 5.5 \times 10^{-10}$ m^2/s.[60] Using the Stokes-Einstein formula for the diffusivity of elongated molecules,[61] we estimated the diffusivity of the surfactant ion for DTAB:

$$(D_1)_{\text{DTAB}} \approx \left[\frac{(\Gamma_\infty^{-1})_{\text{SDS}}}{(\Gamma_\infty^{-1})_{\text{DTAB}}}\right]^{1/2} (D_1)_{\text{SDS}} \tag{B.10}$$

The values of the excluded area per molecule in the adsorption layer, Γ_∞^{-1}, are taken from Table 3 for SDS and DTAB. Thus we obtained $D_1 = 5.0 \times 10^{-10}$ m^2/s for DTAB. The diffusivities of the Na^+, Cl^-, and Br^- ions were calculated from the radii of the hydrated ions[62] with the help of the Stokes-Einstein formula, substituting $\eta = 0.852$ mPa.s for the viscosity of

water at $T = 27°C$. Thus, for the system SDS + NaCl we obtain $D_2 = 7.18 \times 10^{-10}$ m^2/s and $D_3 = 7.83 \times 10^{-10}$ m^2/s, whereas for the system DTAB + NaBr we have $D_2 = 7.83 \times 10^{-10}$ m^2/s and $D_3 = 7.18 \times 10^{-10}$ m^2/s (the hydrated Cl^- and Br^- ions have practically the same size). Afterwards, D was calculated by means of eqs B.1 – B.7 as a function of $c_{1\infty}$ and $c_{2\infty}$.

It should be noted also that the total surfactant adsorption, $\widetilde{\Gamma}_1 = \Gamma_1 + \Lambda_1$, includes both the ions adsorbed at the interface (Γ_1) and the excess ions in the diffuse electric double layer (Λ_1). The computations show that for not too low ionic strengths, $c_{2\infty} \geq 1$ mM, the diffuse electric double layer is relatively narrow, and then Λ_1 is negligible, so that $\Gamma_{eq} = \widetilde{\Gamma}_1 \approx \Gamma_1$. However, at lower ionic strengths ($c_{2\infty} < 1$ mM) one has to substitute $\Gamma_{eq} = \widetilde{\Gamma}_1 = \Gamma_1 + \Lambda_1$ in eqs 5.36 and 5.38; see ref 53 for details.

Appendix C: Dynamic Surface Tension of Micellar Solutions: Derivation of Eq 6.1

For concentrations above the CMC, the initial and boundary conditions for the monomer concentration, c_1, are:

$$c_1 = c_{CMC} \quad \text{at } t = 0 \text{ and } x > 0 \tag{C.1}$$

$$c_1 = c_{CMC} \quad \text{at } t > 0 \text{ and } x \to \infty \tag{C.2}$$

where c_{CMC} is the equilibrium monomer concentration in the considered case. For kinetics of adsorption from micellar surfactant solutions in regimes BC and DE, the diffusion equation and the surfactant mass balance at the interface read:[34]

$$A_L\left(\frac{\partial c_1}{\partial t} - \dot{\alpha} x \frac{\partial c_1}{\partial x}\right) = A_R D \frac{\partial^2 c_1}{\partial x^2} \qquad (t > 0,\ x > 0) \tag{C.3}$$

$$\frac{d\Gamma}{dt} + \dot{\alpha}\Gamma = A_R D \frac{\partial c_1}{\partial x} \qquad (t > 0,\ x = 0) \tag{C.4}$$

where

$$A_L = 1 + \frac{\sigma_{eq}^2}{m_{eq}}\beta, \quad A_R = 1 + \frac{\sigma_{eq}^2}{m_{eq}}\frac{D_m}{D}\beta \quad (\text{regime BC}) \tag{C.5}$$

$$A_L = 1 + \frac{m_{eq}^2 + \sigma_{eq}^2}{m_{eq}}\beta, \quad A_R = 1 + \frac{m_{eq}^2 + \sigma_{eq}^2}{m_{eq}}\frac{D_m}{D}\beta \quad (\text{regime DE}) \tag{C.6}$$

In terms of the variables (y, τ) defined by eq 5.6, eqs C.3 and C.4 acquire the form:

$$A_{\mathrm{L}} \frac{\partial c_1}{\partial \tau} = A_{\mathrm{R}} D t_{\mathrm{age}} \frac{\partial^2 c_1}{\partial y^2} \qquad (\tau > 0,\ y > 0) \tag{C.7}$$

$$\frac{\mathrm{d}}{\mathrm{d}\tau}(\Gamma \widetilde{A}) = A_{\mathrm{R}} D t_{\mathrm{age}} \frac{\partial c_1}{\partial y} \qquad (\tau > 0,\ y = 0) \tag{C.8}$$

Next, we apply Laplace transform to eq C.7 with respect to τ, and solve the obtained ordinary differential equation:

$$L[c_1] = \frac{c_{\mathrm{CMC}}}{s} + L[c_{\mathrm{s}} - c_{\mathrm{CMC}}] \exp[-\frac{(sA_{\mathrm{L}})^{1/2} y}{(A_{\mathrm{R}} D t_{\mathrm{age}})^{1/2}}] \tag{C.9}$$

where L denotes Laplace transform; s is the Laplace parameter; and $c_{\mathrm{s}}(\tau) \equiv c_1(y{=}0, \tau)$ is the subsurface concentration of surfactant monomers. Further, we apply Laplace transformation to eq C.8, and substitute eq C.9:

$$L[\Gamma \widetilde{A}] = \frac{\Gamma_0}{s} - (D_{\mathrm{eff}} t_{\mathrm{age}} / s)^{1/2} L[c_s - c_{\mathrm{eq}}] \tag{C.10}$$

where $\Gamma_0 = \Gamma(\tau{=}0)$ and

$$D_{\mathrm{eff}} \equiv A_{\mathrm{L}} A_{\mathrm{R}} D \tag{C.11}$$

Because eq C.10 is analogous to eq 5.11 in the main paper, we arrive again at eq 5.31, where s_γ is defined by eq 6.1. In addition, the substitution of eqs C.5 and C.6 into eq C.11 leads to eqs 6.4 and 6.5.

The reference numbers are the same as in the main paper; see the reference list therein.